Thermal Analysis and Control of MIST

Anton Björnberg and Erik Larsson

***Abstract*—A thermal analysis has been conducted on the satellite MIST to learn how well different temperature requirements are met in its latest configuration. In the process both a geometrical and a mathematical thermal model have been refined and updated and new information regarding internal heat dissipation has been added. The three thermally most extreme cases have been simulated using the software Systema-Thermica and the results show that several units aboard are not within their temperature limits. Different possibilities to resolve the issues, including the use of passive thermal control, have been discussed.**

I. Introduction

A. Background

SPACE has long been an expensive business, mainly explored by a few wealthy organisations. However, advancements in technology has allowed to miniaturize vital components and paved a way for new space exploring technology, the CubeSats. These are small satellites that are made up of cubic units, each measuring 10 cm $\times$ 10 cm $\times$ 11 cm and allowed a maximum weight of 1.33 kg. CubeSats are mainly used for research purposes and due to the small size, launching costs are extensively smaller for a CubeSat than for a conventional satellite. The cost reductions have opened up the possibility for smaller businesses and universities to venture into space. [1]

By initiative of KTH Space Center, students at KTH Royal Institute of Technology are currently developing the CubeSat MIST (**MI**niature **ST**udent satellite). The objective of the MIST project includes bringing the payload of eight scientific experiments into space orbit, as well as educating students through engineering teamwork. [2] [3]

B. Thermal Analysis of MIST

The thermal conditions in space are very harsh. Deep space has a temperature of 2.7 K, whereas an object exposed to direct sunlight easily can reach several hundred degrees Celsius. As MIST orbits Earth, it will alternate between being in sunlight and being shadowed by Earth, which results in temperature fluctuations. Meanwhile, the temperature of each subsystem and payload aboard are required to stay within certain limits for them to operate correctly. To ensure this, it is necessary to analyze the thermal behaviour of the satellite beforehand and where necessary apply thermal control. [4]

The thermal analysis on MIST has been ongoing since the MIST project was defined in 2015. The initial efforts were made by Andreas Berggren, who used theory of thermodynamics to define an approach on how to mathematically model the satellite's thermal behaviour. He also built a first computer model for simulation with the software Siemens NX. [4]

The work was continued by Shreyas Chandrashekar, who built a comprehensive computer model as new details of the design of the satellite had emerged. It was also decided that the software to be used for simulation would be Systema Thermica, which is developed by Airbus. [5]

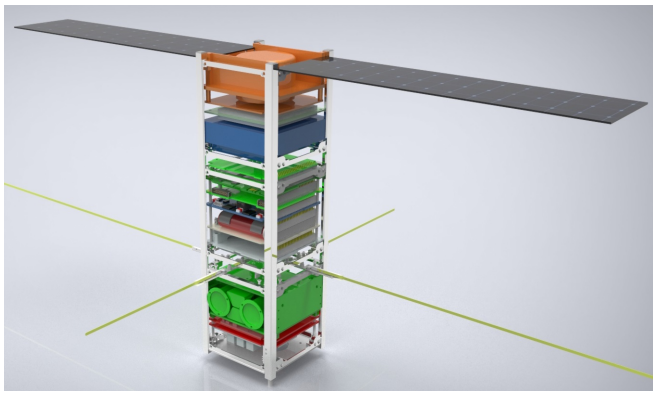

Fig. 1. MIST design without side-mounted solar panels

Furthermore, Jacob Ask Olsson participated by writing a guide for the simulation software, custom tailored for MIST, that would make it easier for new teams to continue the thermal analysis. [6]

C. Goals

New details of the satellite emerge continuously and finalization of the design is coming near. This means that there has been a need to further enhance the model with the most up-to-date information for more accurate and realistic simulations. Thus, the goals of this thesis were the following:

- Update the thermal model to match the most accurate available data
- Investigate how well the thermal requirements are being met
- Investigate some possibilities for thermal control

D. Presentation

The report is organized in the following way:

First is a description of the MIST satellite with its subsystems and payloads. This is followed by a presentation of the thermal theory that has been needed for the simulations, as well as an explanation of the simulation procedure. Next, the results are presented. This includes a description of the updates to the model and the simulation results. Lastly, the results and possibilities of thermal control are discussed and future work is proposed.

II. The MIST CubeSat

The MIST satellite is a 3U CubeSat, which means that it consists of three stacked cubic units and has a total volume

of $10 \times 10 \times 33$ cm^3. The three stacks are referred to as the upper, middle and lower stack respectively and house both the subsystems and payloads. Subsystems are the systems that control vital functions such as power, attitude, data and communication, and the payloads consists of eight scientific experiments. The payloads are fitted in the upper and lower stacks, while most of the subsystems are in the middle stack. The exterior of the satellite will in large part be covered by solar panels. Figure 1 depicts MIST without the side-mounted solar panels.

A. Mission Description.

1) Lifetime and Orbit: MIST is designed to have a lifetime of one year, during which time it will have a sun-synchronous orbit around earth. A sun-synchronous orbit is an orbit where the satellite passes over any point on Earth's surface at the same local solar time [7]. The altitude is set to about 640 km and it will thus make approximately 15 orbits every 24 hours. [8]

2) Detumbling and Attitude: When the satellite first comes into Earth orbit after being launched and separated from the launch vehicle it will rotate around its own axis in an uncontrolled manner, tumbling. In that state it will operate ineffectively. Subsystems aboard will stabilize this rotation in a process called detumbling, until the attitude is fixed in a tower configuration. [2]

3) Dissipation Profile: The systems aboard MIST will not all be operative simultaneously because of technical limitations and the specific scopes of each system. When performing a thermal analysis, it is of importance to know when the systems are operative and not, as they dissipate heat when operative. The collection of information that defines when and where heat dissipation occurs as well as how much heat that is dissipated is called a dissipation profile. [5]

4) Communication: Communication with the satellite is achieved by transferring data with radio waves to and from a ground station located at KTH campus. [2] Communication is only possible when the satellite is close enough to the ground station, which influences when some experiments and subsystems are operative.

5) Material Degradation: Some material properties will change over time as results of for example surface degradations. These are due to effects of accumulated contamination of the surface that in time will increase the absorptivity of the material while the emissivity remains the same [5]. It is common to differentiate the properties at beginning of life (BOL) from the properties at end of life (EOL). The result of the degradation is that temperatures are generally higher in the EOL case and EOL values are therefore used when analyzing the hottest case. For the coldest cases BOL values are used instead.

B. Structure and Subsystems

The structure and subsystems of the satellite are bought off-the-shelf from the suppliers Innovative Solutions in Space (ISIS) and GOMspace. The components are specifically developed for space applications, which means that they are designed to withstand the harsh conditions and should generally not be a concern in a thermal perspective [2]. However, they are included in the analysis for the sake of completeness. Short descriptions of the structure and subsystems components in the MIST satellite are given below. The specific temperature limits for each system are displayed in table I and the location of each system in MIST is displayed in figure 2. The stated limits are for the operative cases, which generally are narrower than the limits for non-operative cases and also are the ones most commonly found in documentation.

1) Printed circuit board (PCB): PCB's are not subsystems of there own, but components that are found in most of the subsystems and payloads on MIST. The purpose of PCB's is to electrically connect electronic components as well as to provide mechanical support. A typical PCB is made up of layers of thin copper sheets separated by insulating material, usually FR-4 glass epoxy and components are usually mounted by soldering [9]. The PCB substrate itself has a high upper temperature limit of about 250°C. However, the components mounted are generally more sensitive and determine the PCB's overall temperature requirements.

2) Structure: The structure for the MIST satellite is the ISIS CubeSat Structural Subsystem. It is built to accommodate the satellite's components, which generally are printed circuit boards in a modular structure. It consists of structural ribs and side frames and are made of aluminum. The surfaces of the side frames are black anodized, which is the driving factor for the thermal requirements of the structural components. [10]

3) On-Board Computer (OBC): The OBC manages and controls all operations on the satellite. It will operate and dissipate heat during the whole time in orbit. [5]

4) Electrical Power System Board (EPS-board): The electrical power system board is in charge of the supply, use and transfer of electrical power. It coordinates the supply of power from the solar panels and batteries to the consumers on the satellite. The board used on MIST is Nanopower P31-us from GOMspace. [5]

5) Batteries: The batteries are needed on a satellite to make sure that the power requirements are met in periods when the solar panels are unable to deliver power, due to for example eclipse or detumbling. The batteries used on MIST are the NanoPower BP4 from GOMspace, which are four lithium ion cells connected to a PCB. It is of grave importance that the batteries do not exceed their temperature limits, which could cause damage and lead to inevitable mission failure. To help with this, the batteries have an integrated heater that is controlled by a temperature sensor. [5]

6) ISIS Generic Interface System (IGIS): IGIS is a group of components that provides a generic interface system to Nano-Satellites. Apart from providing functionality in ground based testing, it also provides connection between the batteries and the internal power system and controls the activation of the deployable systems on the satellite [11]. There are no documented specific thermal requirements for IGIS from ISIS. Instead, an assumption has been made that it has requirements similar to those of other systems equipped with PCB's that are provided by ISIS. The exact limits should be investigated further.

7) Magnetorquer Board (iMTQ): The iMTQ is the component responsible for attitude determination and control, which means keeping the satellite dynamically stable during orbit as well as to detumble it after launch . It is equipped with a 3-axis magnetometer, which measures Earth's magnetic field to determine the satellite's orientation. It also consists of three magnetic torquers, two torque rods and one air core torquer, which together produce the torque that keeps the satellite stable. This is all mounted on a PCB that is operating and dissipating heat constantly. The most sensitive components, in a thermal perspective, are the sensors. [12]

8) TRXVU Transceiver: The TRXVU is a transceiver and is used on the satellite for communication with the ground station. Transceiver is an acronym for transmitter and receiver, and has the highest heat dissipation during transmission. The temperature limits are governed by those of its PCB. [5]

9) Antenna System: The antennas used on MIST are the ISIS deployable ones, which are four shape memory alloy tape antennas connected to a PCB. They are seen in figure 1 as pointing outward from the middle of the satellite. A shape memory alloy is a material that remembers its original shape[13], thus making the antennas easy to transfer on the structure into orbit. The antennas are electrically connected to the rest of the satellite through a PCB, mounted between the middle and lower stack. [5]

10) Solar Panels: The solar panels used on MIST cover almost the entire exterior surface of the satellite. In addition, two deployable solar panels are mounted on the upper stack reaching out from the satellite as can be seen in figure 1. Only one side per panel will be covered with solar cells. However, further technical details of the deployable solar panels are, at the time of writing, very limited and their thermal requirements are assumed to be the same as for the side-mounted ones. They have solar cells that are specifically designed for usage in space. [5]

TABLE I
OPERATIVE TEMPERATURE REQUIREMENTS FOR THE SUBSYSTEMS AND THE STRUCTURE

Subsystem	**Limits [°C]**
OBC	[-25, +65]
EPS	[-40, +85]
Batteries, charging	[-5, +45]
Batteries, discharging	[-20, +60]
IGIS	[-30, +70]
iMTQ, sensors	[-40, +125]
TRXVU	[-40, +60]
Antenna system	[-30, +70]
Solar panels	[-40, +125]
Structure	[-50, +90]

C. Payloads

MIST will carry eight payloads that will conduct different scientific experiments in space. Short descriptions and their thermal requirements are given below. The specific temperature requirements for each payload can be seen in table II.

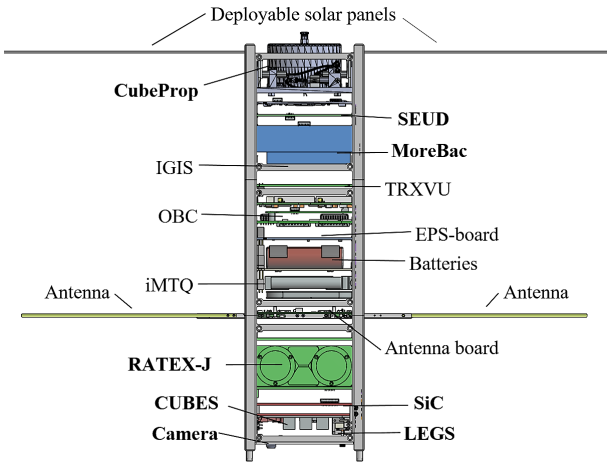

Fig. 2. Location of each system. Payloads are marked **bold**.

The limits differ between the cases when the experiments are operating and not, due to various different causes. The location of the experiments in MIST are displayed in figure 2.

1) Camera: In the nadir direction of the satellite (towards the center of Earth) is a camera situated. It has the goal of capturing and reconstructing high quality images of Earth. The pictures are to be exhibited at Tekniska Museet (Museum of Technology), Stockholm [2]. The exact configuration of the camera is, at the time of writing, not known, but it has been proposed to consist mainly of a PCB connected to a camera module, similar to a Raspberry Pi camera setup. Thus, the temperature limits for the camera on MIST are assumed to be similar to those of the operating temperature limits for a Raspberry Pi camera setup [14]. The exact limits should be investigated further.

2) CUBES: The CUBES experiment will measure the in-orbit radiation environment using three cubic scintillators of different materials. It is developed by the particle and astroparticle department of KTH [5]. When operating, CUBES has a narrow allowed temperature span to avoid calibration errors, but componentwise, the most sensitive components are the sensors located under the scintillators [15].

3) SiC in Space: The SiC in Space experiment is proposed by the Department of Integrated Devices and Circuits at KTH Royal Institute of Technology and will investigate the use of silicon carbide (SiC) in transistors. SiC is a semiconductor material that can be used in integrated circuits operating in harsh environments. The payload consists of a PCB with transistors of different materials, including SiC. The non-operating temperature limits are assumed to be the same as the operating ones, which are the only available limits in the documentation. [16]

4) LEGS: The LEGS experiment is developed by the company PiezoMotor and will investigate the performance of piezoelectric motors in space. Non-operating temperature limits are wide, but when operating the temperature should be between 10 °C and 40 °C for optimal performance of the motor. However, the experiment will likely function for occasional slight exceedances of the limits. The exact details of what is manageable are, at the time of writing, not known.

[17]

5) RATEX-J: RATEX-J is developed by the Swedish Institute of Space Physics in Kiruna, Sweden and is a prototype of a solid state particle detector. The objective of the experiment is to evaluate its performance and efficiency. [2]

6) MoreBac: MoreBac is an experiment that will investigate the growth characteristics of bacteria in a pocket-sized Earth ecosystem in space. The bacteria will be revived from a freeze-dried state and the development of the bacteria will be tracked. MoreBac is developed by the Division of Proteomics and Nanobiotechnology at KTH Royal Institute of Technology [2]. As the bacteria are sensitive, the operating temperature requirements are very narrow and have earlier proven to be difficult to meet [5]. At the time of writing very few technical details are known about MoreBac, so most of the data used in the thermal model are assumptions.

7) SEUD: Radiation might induce undesired effects in most silicon electronic devices. One possible error is single event upsets (SEU) that for example can alter bits from 0 to 1. The objective for the SEUD experiment is to test a self-healing/fault tolerant computer system in space, where the amount of radiation is high. SEUD is developed by KTH Royal Institute of Technology's Department of Electronics and Electronic Systems. [2]

8) CubeProp: CubeProp is a prototype of a propulsion module for CubeSats that is being developed by NanoSpace in Uppsala, Sweden. The module contains a fuel tank that must be thermally controlled so that the fuel does not overheat or freeze during the mission. [2]

TABLE II
TEMPERATURE REQUIREMENTS FOR THE EXPERIMENTS

Experiment	Operating [°C]	Non Operating [°C]
Camera	[0, +70]	[0, +70]
CUBES	25 ± 5	[-20,+80]
CUBES, sensors	[-20, +60]	[-20, +80]
SiC in Space	[-40, +105]	[-40, +105]
LEGS	[+10, +40]	[-30, +70]
RATEX-J	[-20, +20]	[-40, +50]
MoreBac	[+20, +30]	[+4, +30]
SEUD	[0, +85]	[-65, +150]
CubeProp	[0, +40]	[-10, +50]

III. THERMAL THEORY

Heat is defined as thermal energy in transit [18] and can be transferred between systems by three main modes [19], namely conduction, radiation and convection. For a system in space, or more specifically a system in near or complete vacuum, the transfer of energy by convection can be neglected. This makes conduction and radiation the main modes of interest for this report. The theory and equations that are relevant for the simulations are described below.

A. Conduction

Conduction is the transfer of heat due to microscopic collisions between particles. Both within a body as well as in between two bodies, without the displacement of matter. It is governed by Fourier's law, which states that the conduction heat rate q per unit area is proportional to the gradient of the temperature T in the direction normal to the area

$$q = -k\frac{\partial T}{\partial n}. \tag{1}$$

Where k is the proportionality factor given in $\mathrm{W}/(\mathrm{m}\cdot\mathrm{K})$ also known as the thermal conductivity. The negative sign ensures that heat flows from a high to a low temperature. The thermal conductivity k does vary with temperature, but for the temperature ranges involved in this report it can be assumed as a constant.

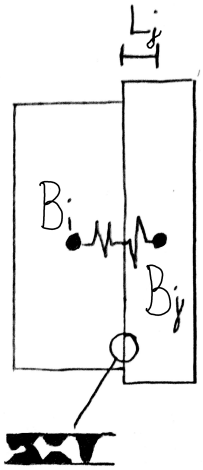

Fig. 3. Conductive coupling and the microscopic contact points related to the thermal contact conductance illustrated. B_j is node j while the cross sectional area A_j goes into the plane.

1) Thermal Contact Conductance: Conduction between two bodies in contact depends on the thermal contact conductance coefficient h_c with unit $\mathrm{W}/(\mathrm{m}^2\cdot\mathrm{K})$ [20]. This takes into account the contact pressure, surface cleanliness and roughness as well as surface deformation. The substantial factor comes from the contact pressure, the harder two materials are pressed together the better heat will flow in between them due to increased contact area. No two materials that are seemingly in full physical contact on a macroscopic level are really in full contact on the microscopical one as seen in Figure 3.

2) Thermal Conductive Couplings: In the MIST project, the satellite is discretized into nodes in accordance with a lumped system analysis, where it is assumed that temperature differences within the specific volume of a node is negligible [20]. The transfer of heat due to conduction between two nodes, B_1 and B_2, is described by the conductive coupling between them. This takes into account the conductance to transfer heat from the middle of each node to its side, as well as the thermal contact conductance. One conductive coupling between the two nodes is then given by

$$GL_{\mathrm{B}_1\to\mathrm{B}_2} = \frac{1}{\frac{1}{G_{\mathrm{B}_1}} + \frac{1}{h_c A} + \frac{1}{G_{\mathrm{B}_2}}}, \qquad \left[\frac{\mathrm{W}}{\mathrm{K}}\right] \tag{2}$$

where h_c is the thermal contact conductance coefficient from above, A is the surface contact area between node B_1 and B_2.

Also

$$G_j = \frac{k_j A_j}{L_j}, \tag{3}$$

where A_j is the cross-sectional area of node j, k_j is the thermal conductivity and L_j is the distance traversed by the heat from the middle of node A_j to the boundary as illustrated in figure 3.

A special case is when B_1 and B_2 does not have interfacing contact surfaces, but rather are sections "of the same piece of material". Then the middle term in the denominator can be neglected, yielding:

$$GL_{\mathrm{B_1}\to\mathrm{B_2}} = \frac{1}{\frac{1}{G_{\mathrm{B_1}}} + \frac{1}{G_{\mathrm{B_2}}}}, \qquad \left[\frac{\mathrm{W}}{\mathrm{K}}\right] \tag{4}$$

B. Radiation

Thermal radiation is energy emitted by matter, and represents a conversion from thermal energy to electromagnetic energy. The energy is then stored in electromagnetic waves and can be transported infinitely if unobstructed [20]. However, when the waves meet matter, the electromagnetic energy can be converted back into thermal energy by absorption [21]. All bodies with a temperature higher than zero kelvin give rise to thermal radiation. The effect of thermal radiation and absorption is for example the heat one feels when standing next to a bonfire, even though the surrounding air could be extremely cold.

Thermal radiation is considered a surface phenomenon for opaque solids [20] and the maximum rate of radiation that a surface can emit is stated by the Stefan-Boltzmann law

$$q = \sigma A T^4 \tag{5}$$

where q is the energy transferred per second, A is the surface area, T is the surface temperature and σ is the Stefan-Boltzmann constant with numerical value $5.67 \times 10^{-8} \frac{\mathrm{W}}{\mathrm{m^2\,K^4}}$. This maximum heat transfer rate is the thermal radiation from an ideal black body. In reality, only part of this radiation is emitted and the ability to radiate is described by the emissivity ϵ. For all real surfaces, the right side of equation (5) must be multiplied by ϵ that varies in the interval $0 \leq \epsilon \leq 1$ and depends on the properties of the surface. The emissivity of a surface then tells how much the surface resembles a black body, which has $\epsilon = 1$.

Another factor that is important is the absorptivity α, which is the fraction of incident radiation energy that is absorbed by the surface,

$$q_{\text{absorbed}} = \alpha q_{\text{incident}}. \tag{6}$$

Radiative Exchange Factor : In analogy to the above discussed conductive coupling the radiative coupling is governed by the radiative exchange factor

$$GR_{B_1\to B_2} = \epsilon_{B_1} D_{B_1\to B_2} A_{B_1}, \tag{7}$$

where ϵ_{B_1} is the emissivity of node B_1, $D_{B_1\to B_2}$ is the Gebhart factor from node B_1 to B_2 and A_{B_1} is the area of the node. The Gebhart factor represents the fraction of energy leaving B_1 being absorbed at B_2 and is a geometrical accountance of the radiative view factor between all nodes seen by B_1. The radiative view factor is the factor between two surfaces describing how much of one the other one sees and hence can radiate with thermal radiation. It is given by

$$F_{B_1\to B_2} = \frac{1}{A_{B_1}} \int_{A_{B_1}} \int_{A_{B_2}} \frac{cos\theta_1 cos\theta_2}{\pi R^2}\, dA_{B_2}\, dA_{B_1}, \tag{8}$$

where $cos\theta_1$ and $cos\theta_2$ is the angle between the normal vectors of the corresponding areas and the line between them with length R.

C. Heat Capacity

Heat capacity is defined by the following equation

$$C = \frac{dQ}{dT}, \qquad \left[\frac{\mathrm{J}}{\mathrm{K}}\right] \tag{9}$$

and describes the amount of energy that is needed to increase the temperature of an object by 1 K [18]. Upon dividing the heat capacity for a given amount of substance by its mass, the material's specific heat capacity c is given. This is a useful quantity that can be used to assign a heat capacity value to every node in the satellite according to

$$C_i = \sum c_j \rho_j V_j. \tag{10}$$

Where C_i is the total heat capacity of node i, c_j is the specific heat capacity, ρ_j the density and V_j the volume of material j within node i.

D. Heat Equation

The heat equation used by the software in this report is

$$\begin{aligned} C_i \frac{dT_i}{dT} =& \sigma \sum_j GR_{ij}(T_j^4 - T_i^4) + \sum_j GL_{ij}(T_j - T_i) + \\ &+ QS_i + QA_i + QE_i + QI_i + QR_i. \end{aligned} \tag{11}$$

Where C_i is the heat capacity, T_i is the temperature of node i, t is the time and the first two sums on the right hand side is described above. The last five terms on the right hand side correspond to different kinds of power sources for node i. QS_i is direct solar radiation power, QA_i is the planet albedo power, QE_i is the planet infra-red power, QI_i is the internal power (from heat dissipation of the components) and QR_i is additional power, also labeled residual flux.

Earth Albedo and Infra-red: Albedo power is the amount of solar power reflected off Earth's surface that strikes a node, whereas the infra-red power comes from the emitted thermal radiation from Earth's surface. Both the albedo and infra-red powers are local phenomena, i.e they are different for different part of Earth's surface. The amount of albedo radiation differ for example if the reflecting surface is water or land.

E. Spacecraft Thermal Control

The purpose of thermal control is to keep a spacecraft's components within their temperature limits [22]. It can be divided into two types, passive and active. Active e.g being electrical heaters that dissipates heat where and when necessary, and demands electrical power. However, due to the

limited amount of electrical power available to the satellite, this is not a practical option for MIST. This brings instead the focus onto what could be done passively, i.e without mechanical moving parts or power consumption. Some options for passive thermal control are described briefly below.

1) Multi-layer Insulation: Multi-layer insulation (MLI) is thermal insulation, with main purpose to reduce thermal radiation and hence isolate a component from its surroundings. This means that both excessive heat loss from the component and excessive heat gain from environmental fluxes is minimized. It is the most commonly used thermal control element on a spacecraft [22]. Generally MLI consists of a blanket composed of multiple layers of low-emittance films that minimize the radiative heat transfer due to reflection. Using low-conductivity, low density spacers between the reflective layers minimizes the conductive transfer, while also making the blanket "fluffy" to minimize contact points [22].

2) Thermal Surface Finishes and Mirrors: Another viable option is the manipulating of surfaces and/or adding of new thin surfaces such as solar reflectors, solar absorbers, flat absorbers and flat reflectors. Manipulating surfaces is mostly achieved by painting or taping a surface to attain a certain emittance or absorptance. While solar reflectors have a high $\frac{\alpha}{\epsilon}$ ratio, absorbers absorb the solar energy while emitting a percentage of the infrared energy. And the flat ones work throughout the spectral range [22]. MLI blankets often have the above named mirrors in various forms, especially on the outer cover layer, where Kapton is a widely used one that has a moderate solar absorptance and a high infrared emittance.

3) Thermal Straps: Thermal straps are used as thermal bridges to distribute heat by conduction, i.e from a warm component to a cold one, or to a good radiative surface where the heat can be rejected. Thermal straps are mainly made by good conductive materials such as copper.

4) Heat Sinks: Heat sinks could be applied to lower the temperature of hot bodies, by attaching a piece of highly conductive material, for example copper. This would lead to lower thermal density due to a greater distribution of heat and could be used to protect components that are sensitive to high temperatures

IV. Simulation and Modelling

A. Simulation

The thermal analysis is carried out by conducting computer simulations of the conditions that the satellite will be subjected to when orbiting earth. The orbit that is used is the MIST reference orbit [7], which is a sun-synchronous orbit at approximately 640×10^3 m altitude. The Software used is Systema-Thermica, henceforth referred to as Thermica. Thermica provides tools for creating a geometrical 3D model of the spacecraft and allows to define a nodal network by meshing. Additional information about for example capacitances and internal dissipations of the satellite are included through a text file that the user provides. In Thermica, it is also required to define the trajectory, attitude and mission specific information to run a simulation.

After a succesful simulation has been carried out, the software can produce a number of different result files, the type of which can be chosen beforehand. In this project the important result files included excel sheets with minimum and maximum temperatures of each node and CSV-files with information of the temperature of each node at each computed point in time.

B. Accuracy and Uncertainty

The accuracy of the results depends on the level of detail of the model and how fine the mesh is. However, as simulation time increases with higher level of detail, it is not practically possible to simulate an fully detailed model. Therefore, the model is a simplification of the real configuration and the number of nodes limited to a manageable level. To account for the uncertainty the simplifications might cause, an additional 10°C are added in each direction to the resulting temperature spans for the analysis. The chosen uncertainty acts as a safeguard and can be adjusted to more realistic values by performing a sensitivity analysis [23] of the model.

C. Simulation Cases

Another limitation that comes with requiring practical simulation times is that not the full lifetime of one year can be simulated. Instead, the most extreme thermal cases are simulated individually. Since the temperature limits of the systems varies depending on them being operative or not, this leads to three different simulation cases that are described below. If temperatures are kept within the allowed limits in these three cases, it can be guaranteed that the thermal requirements are met also in every other case.

1) Hot Case, Operational: This case corresponds to conditions that produce the highest temperatures the satellite will be subjected to and occurs at the time of the year when Earth is approximately closest to the sun, which is at winter solstice. In this case all subsystems and payloads are operational, meaning that they might dissipate heat and the operational temperature requirements apply. Also, the effect of surface degradation is applied. This means that the satellite has been subjected to space radiation and values for absorptivity and emissivity may differ from other cases [5]. Generally surface degradation increases the absorptivity for materials, thus appropriate for the hot case.

2) Cold Case, Operational: This case differs from the hot case in that it occurs at the time of the year when Earth is situated approximately the furthest from the sun, which corresponds to summer solstice. No degradation is applied as to make it a worst case scenario for the cold case and BOL values are used. Therefore here the satellite will be subjected to the lowest temperatures possible with the operational temperature requirements. [5].

3) Cold Case, Non-Operational: This case also occurs during summer solstice. However, no experiments are operational so that the total internal dissipation is lower than in the other cases. Thus, the temperature requirements corresponds to those given for non operational states of the experiments and the temperatures will be the lowest of all the three cases.

D. The Thermal Model

The thermal model consists of two main parts, one geometrical and one mathematical.

1) Geometrical Model Management: The geometrical model management (GMM) is handled in Thermica, where a geometrical model is built in accordance with a CAD (computer aided design) drawing of MIST. However, the amount of detail in the thermal model is greatly reduced in comparison to the CAD drawing to reduce simulation times. The geometrical model consists mostly of rectangles and a few cylinders where appropriate. On top of this is the meshing defined to divide the satellite into nodes. The geometrical model with its meshing is displayed in Figure 4 . Values for emissivity and absorptivity, as defined in section III-B, are manually set for each surface. With these data, Thermica can calculate the radiative exchange factor, as defined in equation (7), between the nodes and the power absorptions from the thermal radiation between the nodes and their environment. It is done via the Monte-Carlo Ray tracing method, which is a method that uses randomness to calculate deterministic values with high accuracy [24].

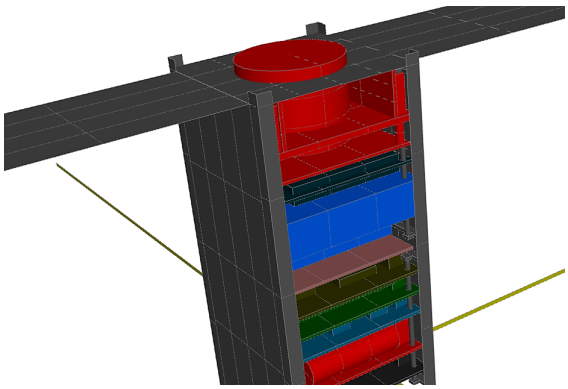

Fig. 4. Part of the geometrical model with applied meshing

2) Thermal Mathematical Management (TMM): Apart from the radiation exchange in equation (11), Thermica requires information about the heat capacity of each node and the conductive couplings between all the nodes to run accurate simulations. This is managed in an excel file referred to as the TMM. In this, the mathematical properties of each node are defined and include their specific heat capacity, density, conductivity and physical dimensions. For overview and reference purposes, the surface treatment and hence a node's emissivity and absorptivity are also found in the TMM. This is then used in the TMM to calculate the capacitances and all the conductive couplings between the nodes in accordance to equations (9) and (2). The TMM also produces the code necessary for Thermica to use the calculated data. The code is included in a text file, referred to as a user file, and is used by the solver, also called Thermisol, in Thermica during simulation.

V. Model Changes

In the project, several updates and changes have been made to the GMM and the TMM. The main ones are described in this section.

A. M3 Bus Spacers

Each cubic unit of MIST is held together by four rods running through the corners of the payloads and subsystems. Between each "floor" of the satellite, each rod is encapsulated by a M3 bus spacer, as shown in figure 5. The volume in-between the bus spacer and the rod is filled with vacuum, which means that the amount of heat conducted directly to the rod is negligible. In addition, the bus spacers have contact interfaces at the ends. All this adds up to a significant impact on the ability of heat to flow in the direction of the rods. In the previous model each "floor" in the thermal model had thermal couplings directly to the rods, which do not correspond well to reality and consequently was changed.

In the new model the rods are omitted and instead only the bus spacers are taken into account. The conductance are calculated using formulas (2) and (3). The inner radius is 1.6 mm and the outer radius is 2.5 mm , so the cross sectional area becomes

$$\pi(2.5^2 - 1.6^2)\ \text{mm}^2 \approx 11.59\ \text{mm}^2.$$

The material is Aluminum 1050A and the height varies between the "floors" in the satellite. In addition, the connecting M3 Female AL standoffs seen at the top in Figure 5 were also implemented and calculated in the TMM.

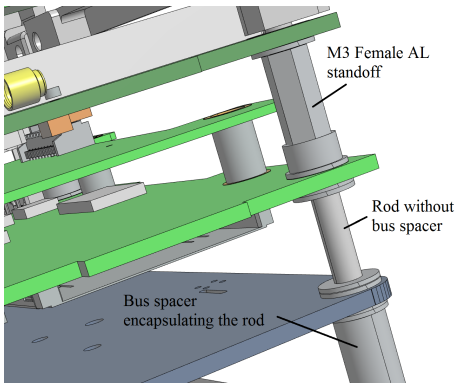

Fig. 5. Rods are encapsulated by bus spacers

B. Printed Circuit boards (PCB's)

Many components on MIST are PCB's. These are described in section II-B1 and are made up of layers of thin copper sheets separated by an insulating material, usually FR-4. The nature of the design means that heat is conducted differently when considering conduction in-plane versus through-plane. This differentiation in direction has been implemented in the TMM excel file. A table has also been added in a separate tab ("PCB Data"), where data of each PCB in MIST is manually entered. The necessary input data includes the number of copper layers, the thickness of the copper layers and the total thickness of each PCB. With this information it is possible to calculate the conductive couplings for the PCB's in the two directions under certain assumptions.

1) In-plane: The conductivity for copper (401 W/(m·K)) is about 500 times larger than that of FR4 (0.53 W/(m·K)). Therefore conduction through the FR4 is neglected, and the conductance is calculated as the one of a single sheet of copper with a thickness corresponding to the total thickness of all the copper layers in the PCB.

2) Through-plane: The conduction through-plane is governed to the largest part by the insulating material as it constitutes about 99.99% of the total thickness in a typical PCB in MIST. Thus, the conductance through-plane is calculated as the one of a single piece of FR4 with the same dimensions as the PCB.

C. Emissivity and Absorptivity

Values for emissivity and absorptivity has been updated for several components as new technical details have become known. Some of the earlier values were approximations or assumptions. Components that have been updated include the following:

- Deployable solar panels
- Rods and bus spacers
- Side frames and structure ribs
- The scintillators in CUBES
- Bearingholder module on LEGS
- Magnetorquer (iMTQ)

D. Internal Dissipation Profiles and Trajectory

New dissipation profiles have been defined to match the latest profile given by the power management subteam on MIST. Figures 6 and 7 show the internal dissipations during the simulations for the cold, operational case.

In the non operational case the experiments have zero dissipation, but the profile for the subsystems looks the same, apart from dissipation of the battery. The battery has an integrated heater that is active when the battery is in risk of becoming too cold. The dissipation of the battery might therefore vary from simulation to simulation.

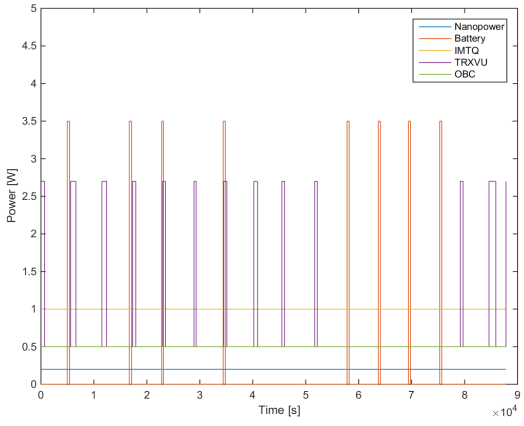

Fig. 6. Dissipation time profile for subsystems

Refinements have also been made in terms of how the dissipations are distributed over the components. Previously, the dissipations were assumed to happen uniformly over each component, e.g if the SEUD PCB was dissipating 0.8 W every node on the PCB would share an equal amount of these 0.8 W. The dissipation distributions have been refined according to available information. The components that were updated in this manner are listed below.

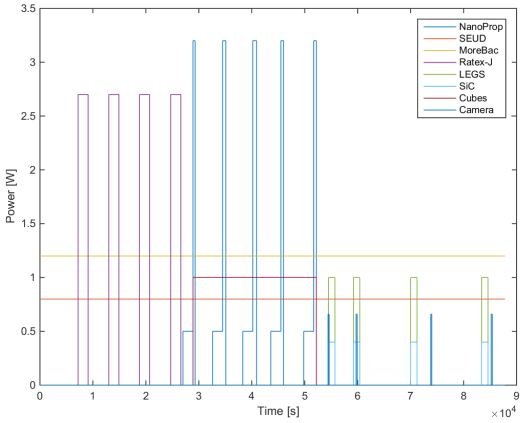

Fig. 7. Dissipation time profile for experiments

1) SEUD: For SEUD a total dissipation power of 0.8 W is distributed to the nodes where the two field-programmable gate arrays (FPGA's) and the power conditioning are located on the PCB. The total is split into 10 % for the power, and 60 % and 30 % respectively for the two FPGA's. This geometrical distribution is in accordance with approximations made by the experiment developers.

2) CUBES: For CUBES 90 % of the total dissipating power of 1.0 W originates from the FPGA that is mounted on the PCB. However, the exact location of the FPGA is not known so for the model the dissipation has been set onto an arbitrary node not occupied by the scintillators themselves. The rest of the dissipation power is assumed to be used for power conditioning and is distributed onto an opposite node.

3) TRXVU Transceiver: The dissipation for the TRXVU transceiver is modeled with a hotspot at the node where the radio frequency power amplifier is located. During transmission, i.e when the satellite is over the ground station, this node dissipates 2.7 W. During the rest of the orbit a uniformly distributed dissipation of 0.5 W is applied, as transceiver is in static operation in that time.

4) OBC: For the OBC an assumed distribution of the total dissipation of 0.5 W between the motherboard and daughterboard is made, with 70 % and 30 % on the motherboard and daughterboard respectively.

Some changes are also made to the trajectory description in Thermica to synchronize the satellite's position and the start time for the dissipations given.

E. Interfacing Surfaces

The thermal contact conductance coefficient, h_c, plays a major part in the conductive coupling between two interfacing nodes originating from different solids in the model. Hence

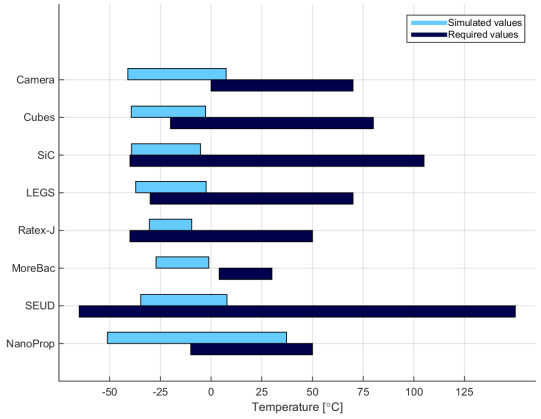

Fig. 8. Temperature ranges for the cold non-operational case, payloads.

this makes it an important factor that should not be neglected when appropriate values for it can be set. Due to its dependence on so many factors, as described in section III-A1, this can be a difficult task and many interfacing surfaces lacked the h_c factor in their conductive couplings prior to this report.

In discussion with the supervisor as well as considering a couple of experimental studies related to the specific materials, a thermal contact conductance coefficient value has been approximated and implemented for the following interfacing surfaces.

- Side frames and structure ribs
- Bus spacers on the main structure and the interfacing PCB's as well as the structure ribs
- Bus spacers on the OBC between motherboard and daughter board

Worth mentioning is that the couplings that these are part of are going to be tested later through a thermal vacuum test to confirm the values. The current approximations are based upon estimating how hard the surfaces will be bolted together i.e the pressure between them.

VI. Results

The results from the simulations are shown in figures 8 to 13 and in tables III to VIII. The plots display the temperature ranges that the subsystems and payloads were subjected to during the simulation of 15 orbits, which corresponds to one full day. All temperature ranges presented here include uncertainties to account for modelling errors. These are 10°C for all systems except for the battery, which has a lower uncertainty of 3°C. This is due to it having its lower temperature controlled by an integrated heater. In the figures one can see if the component at any time during the orbit has exceeded its required range. Tables are also presented with numerical values of these extremes. For detailed plots displaying the varying temperature as a function of time the reader is referred to the appendix. Note that DSP and SSP in the figures refer to deployable and side-mounted solar panels respectively.

TABLE III
Temperature ranges of the payloads for the cold non-operational case and their status

Cold Non-Operational		**Temperature (°C)**		**Status**
		Min	**Max**	
Camera	Simulation	-41	7.4	Cold
	Limits	0	70	
CUBES	Simulation	-39.3	-2.7	Cold
	Limits	-20	80	
SiC	Simulation	-39.2	-5.2	Ok
	Limits	-40	105	
LEGS	Simulation	-37.2	-2.4	Cold
	Limits	-30	70	
RATEX-J	Simulation	-30.4	-9.5	Ok
	Limits	-40	50	
MoreBac	Simulation	-27.1	-1.1	Cold
	Limits	4	30	
SEUD	Simulation	-34.7	7.9	Ok
	Limits	-65	150	
CubeProp	Simulation	-51.1	37.2	Cold
	Limits	-10	50	

TABLE IV
Temperature ranges of the subsystems for the cold non-operational case and their status

Cold Non-Operational		**Temperature (°C)**		**Status**
		Min	**Max**	
Antennas	Simulation	-53.8	31.7	Cold
	Limits	-30	70	
OBC	Simulation	-17.6	23.3	Ok
	Limits	-25	65	
TRXVU	Simulation	-25.1	40.6	Ok
	Limits	-40	60	
iMTQ	Simulation	-7.4	28.8	Ok
	Limits	-40	125	
Battery	Simulation	-5.1	29.1	Cold
	Limits	-5	45	
Nanopower	Simulation	-14.5	18	Ok
	Limits	-40	85	
IGIS	Simulation	-26	19.5	Ok
	Limits	-30	70	
Structure	Simulation	-52.5	37.4	Cold
	Limits	-50	90	
SSP	Simulation	-50.7	19	Cold
	Limits	-40	125	
DSP	Simulation	-60.3	54.9	Cold
	Limits	-40	125	

TABLE V
TEMPERATURE RANGES OF THE PAYLOADS FOR THE COLD OPERATIONAL CASE AND THEIR STATUS

Cold Operational		Temperature (°C)		Status
		Min	Max	
Camera	Simulation	-37.7	18.4	Cold
	Limits	0	70	
CUBES	Simulation	-36.1	23.4	Cold
	Limits	20	30	
SiC	Simulation	-34.1	15.4	Ok
	Limits	-40	105	
LEGS	Simulation	-33.7	20.9	Cold
	Limits	10	40	
RATEX-J	Simulation	-21.2	32.2	Cold and
	Limits	-20	20	hot
MoreBac	Simulation	-3.7	23.2	Cold
	Limits	20	30	
SEUD	Simulation	-6.9	35.9	Cold
	Limits	0	85	
CubeProp	Simulation	-47.8	41.9	Cold and
	Limits	0	40	hot

TABLE VI
TEMPERATURE RANGES OF THE SUBSYSTEMS FOR THE COLD OPERATIONAL CASE AND THEIR STATUS

Cold Operational		Temperature (°C)		Status
		Min	Max	
Antennas	Simulation	-50.9	34.1	Cold
	Limits	-30	70	
OBC	Simulation	-14.4	26.4	Ok
	Limits	-25	65	
TRXVU	Simulation	-20.5	44.1	Ok
	Limits	-40	60	
iMTQ	Simulation	-5.5	31.5	Ok
	Limits	-40	125	
Battery	Simulation	-4.3	27.1	Ok
	Limits	-5	45	
Nanopower	Simulation	-13.4	21.1	Ok
	Limits	-40	85	
IGIS	Simulation	-21.2	23.3	Ok
	Limits	-30	70	
Structure	Simulation	-49.7	40.9	Ok
	Limits	-50	90	
SSP	Simulation	-47.1	23.7	Cold
	Limits	-40	125	
DSP	Simulation	-58.7	56.4	Cold
	Limits	-40	125	

TABLE VII
TEMPERATURE RANGES OF THE PAYLOADS FOR THE HOT OPERATIONAL CASE AND THEIR STATUS

Hot Operational		Temperature (°C)		Status
		Min	Max	
Camera	Simulation	-26.7	37.9	Cold
	Limits	0	70	
CUBES	Simulation	-24.4	40.4	Cold and
	Limits	20	30	hot
SiC	Simulation	-22.7	32	Ok
	Limits	-40	105	
LEGS	Simulation	-21.3	37.9	Cold
	Limits	10	40	
RATEX-J	Simulation	-7.3	46.1	Hot
	Limits	-20	20	
MoreBac	Simulation	9.5	39.6	Cold and
	Limits	20	30	hot
SEUD	Simulation	3.4	51.9	Ok
	Limits	0	85	
CubeProp	Simulation	-41	54.2	Cold and
	Limits	0	40	hot

TABLE VIII
TEMPERATURE RANGES OF THE SUBSYSTEMS FOR THE HOT OPERATIONAL CASE AND THEIR STATUS

Hot operational		Temperature (°C)		Status
		Min	Max	
Antennas	Simulation	-43.9	47.9	Cold
	Limits	-30	70	
OBC	Simulation	-3.5	49.7	Ok
	Limits	-25	65	
TRXVU	Simulation	-9.4	68.2	Hot
	Limits	-40	60	
iMTQ	Simulation	5.8	46.1	Ok
	Limits	-40	125	
Battery	Simulation	7.2	36.4	Ok
	Limits	-5	45	
Nanopower	Simulation	-2.2	39.3	Ok
	Limits	-40	85	
IGIS	Simulation	-10.1	48.2	Ok
	Limits	-30	70	
Structure	Simulation	-43	57.6	Ok
	Limits	-50	90	
SSP	Simulation	-39	45.6	Ok
	Limits	-40	125	
DSP	Simulation	-54.3	71.1	Cold
	Limits	-40	125	

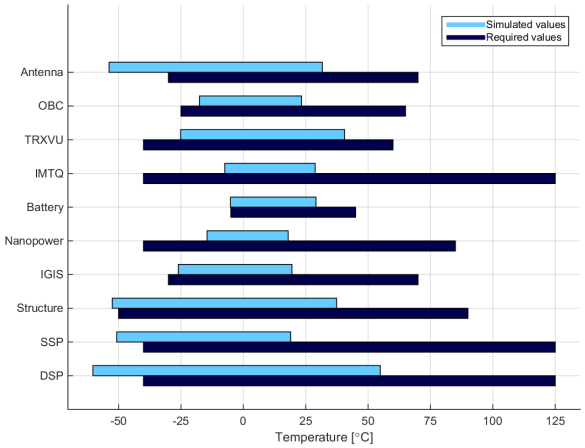

Fig. 9. Temperature ranges for the cold non-operational case, subsystems. SSP are the solar panels on the sides, DSP are the deployable ones.

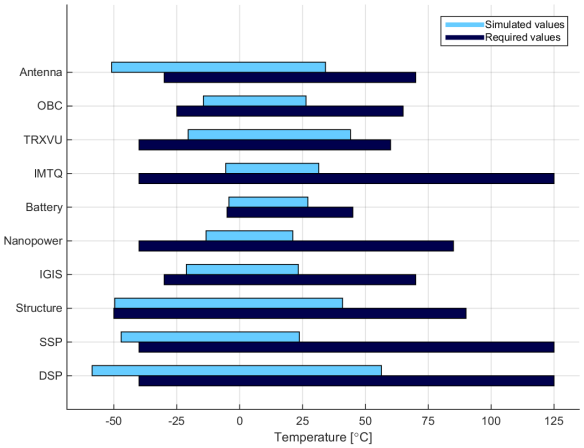

Fig. 11. Temperature ranges for the cold operational case, subsystems. SSP are the solar panels on the sides, DSP are the deployable ones.

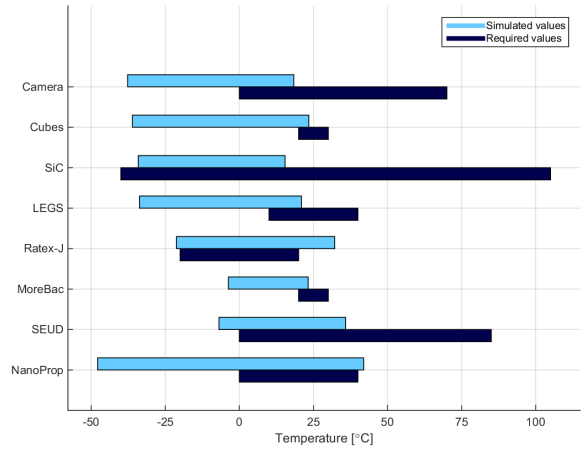

Fig. 10. Temperature ranges for the cold operational case, payloads.

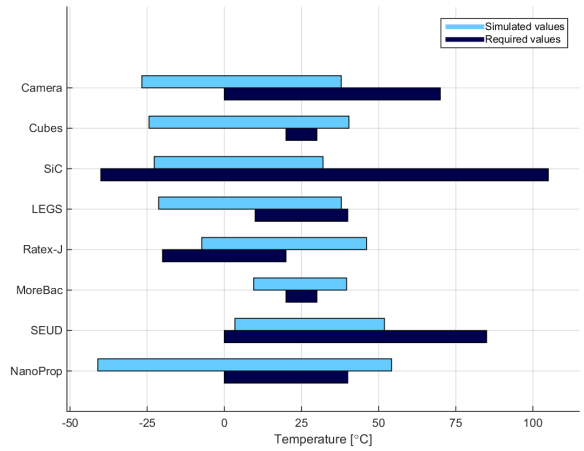

Fig. 12. Temperature ranges for the hot operational case, payloads.

VII. Analysis and Discussion

The results show that many temperature limits are exceeded. Each system is discussed separately in this section.

A. Subsystems

In figures 9, 11 and 13 and tables IV, VI and VIII the simulation results for the subsystems are displayed. It is seen that 18 of the 30 cases are found to stay within the allowed limits. Generally the exceedances are also smaller for the subsystems than for the payoads. However, the results include an assumed modelling uncertainty of $\pm$ 10°C. By performing a sensitivity analysis this uncertainty could possibly be reduced enough for some ranges to fall within the limits. Nevertheless, the deployable solar panels and the antenna system surpasses their lower limits with between about 14°C and 24°C in every case, which means that reducing the uncertainty would not be enough to bring them within their limits.

The reason that these systems do not meet their requirements might be that they reach far out from the larger mass of the satellite. Also, by having large surface areas in relation to their masses they are able to emit significant thermal radiation, lowering the temperatures. The distance to the rest of the satellite decreases the amount of heat from internal dissipation that can reach them.

Since the solar panels only have solar cells fitted on one side, it might be possible to alter the surface treatment on the backside, lowering the emissivity for better heat conservation.

It is also worth noting that the temperature limits used for IGIS are not verified by ISIS and may not be correct.

B. Camera

The camera is seen to exceed its required lowest temperature in all three cases and by a substantial amount as well. This is probably due to it being on the end of the satellite, furthest away from the components which are turned on continuously thus creating heat in the satellite. It is seen in figures in the appendix to be more stable within its limits when nearby components, such as the CUBES experiment, are turned on.

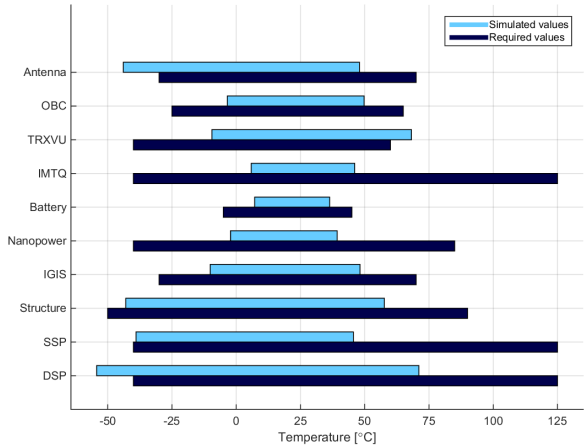

Fig. 13. Temperature ranges for the hot operational case, subsystems. SSP are the solar panels on the sides, DSP are the deployable ones.

The non-operating temperature requirements used here are based on assumptions, but if proper requirements could be found, an idea is to have the camera operating only in those warmer periods. This could be a viable option due to the camera not operating for a long period of time and its competition in the power demand is relatively low. Finally, the camera's temperature requirements might change when the final camera configuration has been decided upon.

C. CUBES

CUBES is having a hard time staying within the very narrow temperature requirements while operating and is also going below the desired non-operational temperature of -20°C. Due to CUBES not facing the Sun nor the Earth its received heat flux is negligible and the sensors directly under the scintillators are in risk even when not operating. While the operating temperature could be above a general working temperature for the electronics when CUBES is on, it is fluctuating to much to stay within the required interval. Since the motivation for operating limits is to avoid temperature calibration errors, another approach for the experiment could be to measure the temperature when operating and account for the temperature fluctuations in the post-processing of the collected data. This could lead to thermal requirements that are easier to meet. Also, a sensitivity analysis could be helpful here.

Due to the scintillators themselves being so small, the options for manipulation of their emittance are very limited and would in accordance to (5) save what might be an insufficient amount of energy. But this amount of energy kept within the system, with a MLI approach could be a possibility. However, CUBES is deemed hard to passively thermally control.

D. SiC in Space

The SiC in space experiment is found to stay within its temperature limits in all cases.

E. LEGS

The LEGS experiment is found to surpass its lower temperature in every simulated case. It exceeds the limit by between about 7°C and 44°C depending on the case. It is seen in figures in the appendix that LEGS is experiencing higher temperatures during the operating time of CUBES in orbit 6 to 10, even spending most of its time within the required range during the hot case. LEGS being mounted close to CUBES on the satellite could take advantage of this and change its operating schedule to coincide with CUBES if possible. From a thermal perspective this might be a solution. Then, even if LEGS is subjected to lower temperatures than the required ones when not operating, it could operate in the periods when temperatures are higher.

LEGS has also not been refined in terms of where the heat dissipation takes place, which otherwise could be beneficial to achieve more realistic simulations. However due to LEGS' short running time in comparison with CUBES, the biggest heat gain is when CUBES is operating.

In addition, the stated limits for LEGS are only those that gives optimal performance, and it is said to still function for some temperatures outside of these. The exact limits of what is manageable should be investigated further. A sensitivity analysis could also possibly reduce the uncertainty and bring the simulated temperatures closer towards allowed limits.

F. RATEX-J

The RATEX-J experiment is found to exceed its limits in the operational cases. The largest exceedances are towards the higher limits. It can be seen in figures the in appendix, that the cause for this might be accumulated heat when operating. The module does not cool fast enough between its operative cycles. One option to solve this could be for the experiment to run less frequently, giving it more time to cool. Another option could be to alter the surface treatment of the module to achieve higher emissivity and faster cooling. Also, adding a heat sink to increase the thermal mass could be an option that could lower the highest temperature of the module.

G. MoreBac

The MoreBac experiment fails to stay within its boundary temperatures in all simulated cases. Due to the narrow allowed span of 10°C when operating and the total uncertainty span of 20°C that is added on top of the simulated range, it is somewhat an impossible task to achieve satisfying temperatures. However, as very little information about the experiment is known, and most of its modelling is based on assumptions, these result will probably be subjected to change when more information becomes available and more accurate simulations can be made. Still, it will remain a difficult task to keep the temperatures within the currently required limits and it should be further investigated if they can be widened.

H. SEUD

The SEUD experiment is found to stay within its temperature limits in all but the cold operational case. Figures in

the appendix shows that the fluctuations are relatively stable and in a majority of the time the temperature is within the required limits. It could be investigated more closely what effects these occasional exceedances might cause to determine if they could be manageable. A sensitivity analysis could be performed to adjust the uncertainty, which could reduce the exceedance levels. If the uncertainty is reduced by at least about 7°C, SEUD would meet the thermal requirements.

I. CubeProp

CubeProp is deemed an extremely difficult experiment to keep within its temperature requirements. It is seen becoming too hot as well as too cold. Being on top of the satellite the tank is receiving a relatively large amount of solar power which is deemed good or bad depending on which case it is. It is also seen in figures the appendix, that CubeProp as a whole component is not that disturbed in its temperature periodicity by the actual running of the experiment and the 30 minutes of pre-heating by the heater designated to bring the tank to within certain temperature limits before running the experiment. So the going in and out of eclipse, i.e seeing the Sun is the driving factor for the temperature of CubeProp. However, due to lack of information regarding the geometric dissipation at the time of simulations, all the heating power as well as running power is modelled to be distributed onto the whole experiment uniformly. Since the tank is the most sensitive component a more realistic geometric dissipation is preferable for a better analysis. The heater should be located below the tank and the driving thruster chips are located on the two PCB's seen at the tank's left and right-hand side in Figure 2. As soon as the exact location of these are known the model should be updated and re-simulated.

After implementing these refinements, it could be possible to manipulate how the thermal energy from the Sun is absorbed and distributed between CubeProp's components and its surroundnings by passive thermal control.

VIII. Conclusion

In this thesis the thermal modelling of the MIST satellite has been refined and updated in order to achieve more realistic simulations. The three thermally most extreme cases were simulated with the updated model and the results show that several of the payloads and subsystems fail to meet their thermal requirements.

Some of the issues could possibly be resolved by performing a sensitivity analysis and implementing passive thermal control, but others seem to offer significant difficulties with the current requirements. This is especially the case for MoreBac and CUBES, whose operating temperature limits are exceeded by the simulation uncertainty alone. For these experiments further investigation should be made to see if the requirements can be reassessed.

On the whole MIST is, with its current configuration, not safe to operate in space without a significant risk of mission failure due to thermal issues.

IX. Future Work

Suggestions for future work within thermal analysis of MIST is collected here.

A. Sensitivity Analysis

In accordance with the discussions held above, a sensitivity analysis should be made to investigate more closely what uncertainties are reasonable to apply to the results from the simulations. This could possibly decrease the resulted temperature spans that are presented and lead to more requirements being fulfilled.

B. Tumbling Case

In the very beginning of its lifetime MIST will encounter tumbling, which does not correspond to any of the cases simulated in this thesis. The thermal conditions in the tumbling case are likely to differ from these and should therefore be investigated separately to ensure that the thermal requirements are met in that case as well.

C. Further Refinements of the Model

Due to lack of documentation, several properties in the modelling of the payloads and subsystems are only assumptions and should be updated when verifiable information is available for more realistic simulations. For a detailed intel into how the assumptions are made, the TMM should be studied. The systems that are most affected by assumtions are MoreBac, the camera and the deployable solar panels.

For CubeProp and LEGS the above discussed refining of the experiments modeling should be done. As well as for CubeProp establishing a more detailed dissipation profile in regards to how the experiment will be conducted and how much power it will use when it is operating is needed. CubeProp is in the results presented in this thesis assumed to run on the mode that uses the most power from the power team, which from a thermal perspective is not necessarily the most realistic nor most extreme one, depending on the case considered.

One might also want to systematically compare the latest updated CAD model of MIST, with the geometrical model in Thermica to check for alikeness. Especially as CubeProp has received an updated design that has been delivered to the mechanical subteam, which has to be changed in Thermica anyway.

D. Thermal Control

In section VII several suggestions are made to how the thermal requirements could be achieved by applying passive thermal control. The possibilities of implementing thermal control and the impact it would have could be further investigated in order to better meet the thermal requirements.

E. Update the Thermal Requirements

The results in this thesis make it clear that many systems are within their allowed temperature ranges in the majority of the time, but occasionally exceeds it. It could be further investigated the effects of occasional exceedances to determine if the systems could withstand such conditions and consequently possibly update the thermal requirements to account for this.

ACKNOWLEDGMENTS

The authors would like to thank Andreas Berggren and Sven Grahn for their valuable guidance and assistance throughout the project.

REFERENCES

[1] (2017, April) Cubesat. [Online]. Available: https://en.wikipedia.org/wiki/CubeSat
[2] MIST, *MIST Project Handbook*, 3rd ed., KTH, Stockholm, December 2016.
[3] A. Gårdebäck. (2017, April) Studentsatelliten MIST. [Online]. Available: https://www.kth.se/sci/centra/rymdcenter/studentsatellit/studentsatelliten-mist-1.481707
[4] A. Berggren, "Design of Thermal Control System for the Spacecraft MIST," Master's thesis, KTH, 2015.
[5] S. Chandrashekar, "Thermal Modelling and Design of MIST CubeSat," Master's thesis, KTH, 2016.
[6] J. A. Olsson, *Thermal control of MIST: A User-Friendly Guide to Thermica and the Thermal Control of the MIST-spacecraft*, December 2016.
[7] MIST, *MIST Reference Orbit*, 3rd ed., KTH, Stockholm, April 2015.
[8] *MIST System Design File*, 2nd ed., KTH, Stockholm, June 2016.
[9] (2017, April) Printed Circuit Board. [Online]. Available: https://en.wikipedia.org/wiki/Printed_circuit_board
[10] MIST, *STS Interface Specification*, 2nd ed., KTH, Stockholm, December 2012.
[11] ——, *ISIS Generic Interface System Datasheet*, 1st ed., KTH, Stockholm, March 2011.
[12] ——, *iMTQ Interface Control Document*, 1st ed., KTH, Stockholm, April 2015.
[13] A. I. H. Committee, *Properties and Selection: Nonferrous Alloys and Special- Purpose Materials*, ser. Metals handbook. ASM International, 1990.
[14] (2017, April) Raspberry Pi camera operating temperature. [Online]. Available: https://www.raspberrypi.org/help/faqs/performanceOperatingTemperature
[15] "Thermal interface meeting," February 2017.
[16] MIST, *Interface Control Document - SICIS*, 4th ed., KTH, Stockholm, December 2016.
[17] ——, *Interface Control Document - LEGS*, 4th ed., KTH, Stockholm, December 2016.
[18] S. J. Blundell and K. M. Blundell, *Concepts in Thermal Physics*. Oxford, United Kingdom: Oxford Univ. Press, 2009, ch. 2.
[19] R. D. Karam, *Satellite Thermal Control for Systems Engineers*. Virginia: American Institute of Aeronautics, Inc., 1998, ch. 2.
[20] Y. A. Cengel, *Heat Transfer : A Practical Approach*. Texas: Mcgraw-Hill, 2002.
[21] W. West. (2017, April) Absorption of Electromagnetic Radiation. [Online]. Available: http://accessscience.com/content/absorption-of-electromagnetic-radiation/001600
[22] G. et al, *Spacecraft Thermal Control Handbook, Volume 1: Fundamental Technologies*. Virginia: American Institute of Aeronautics and Astronautics, Inc, 2002.
[23] (2017, April) Sensitivity Analysis. [Online]. Available: https://en.wikipedia.org/wiki/Sensitivity_analysis
[24] (2017, April) Monte Carlo Method. [Online]. Available: https://en.wikipedia.org/wiki/Monte_Carlo_method

APPENDIX
DETAILED PLOTS

Here are more comprehensive plots displaying the dissipation profiles and the simulation results presented. The latter display the simulated temperatures over the whole simulation time. Each plotted curve in these correspond to the nodes in the geometrical model that are associated to each system. Also lines marking the temperature limits for the system and the maximum and minimum temperatures including uncertainties are included.

A. *Cold case, non operational*

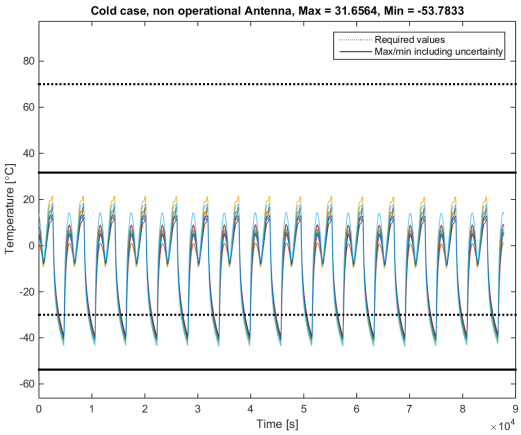

Fig. 14. Cold case, non operational Antenna

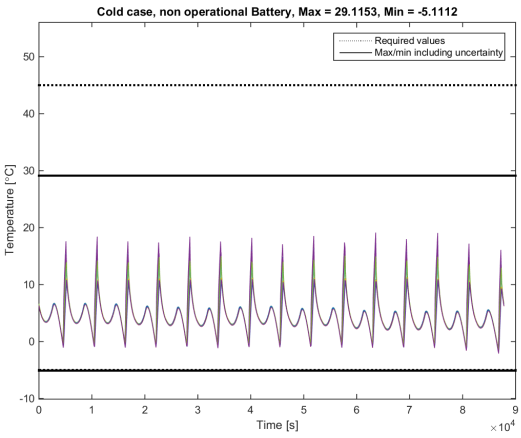

Fig. 15. Cold case, non operational Battery

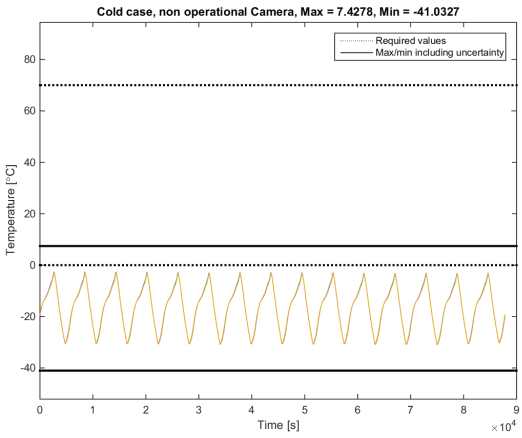

Fig. 16. Cold case, non operational Camera

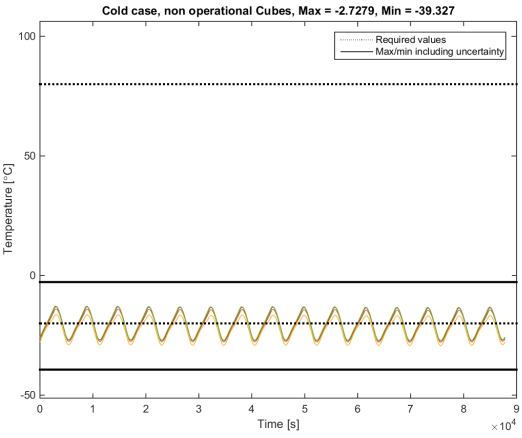

Fig. 17. Cold case, non operational Cubes

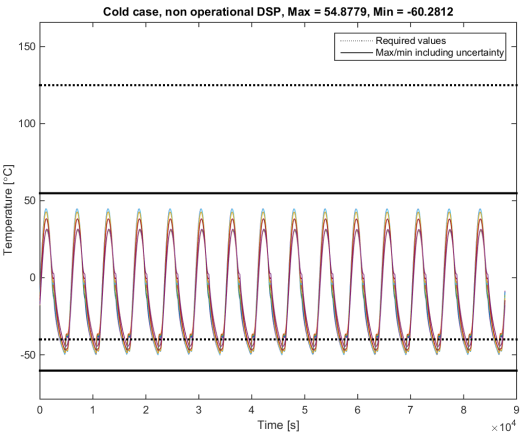

Fig. 18. Cold case, non operational Deployable solar panels

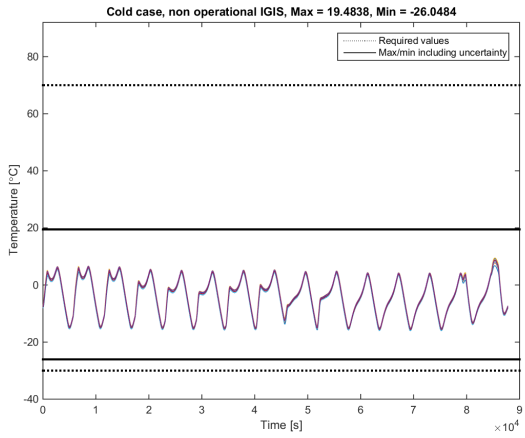

Fig. 19. Cold case, non operational IGIS

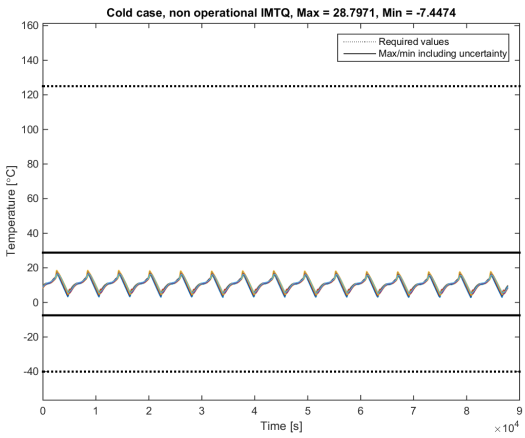

Fig. 20. Cold case, non operational IMTQ

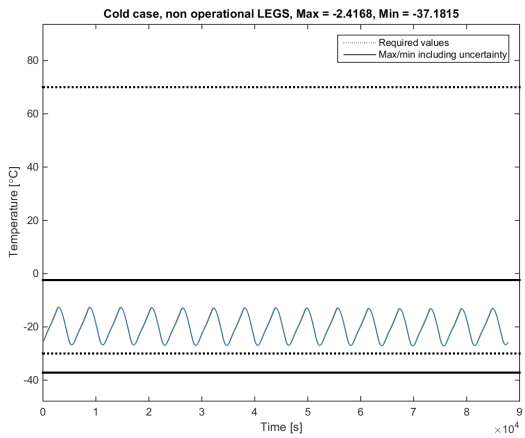

Fig. 21. Cold case, non operational LEGS

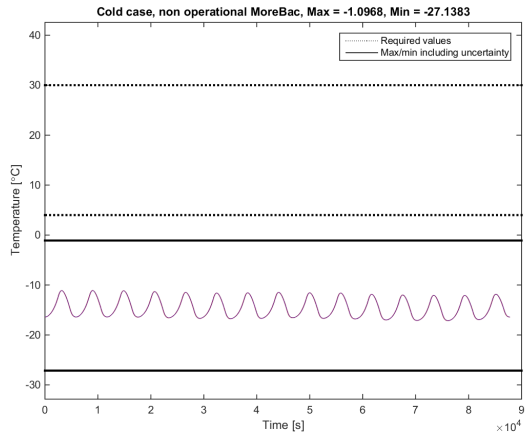

Fig. 22. Cold case, non operational MoreBac

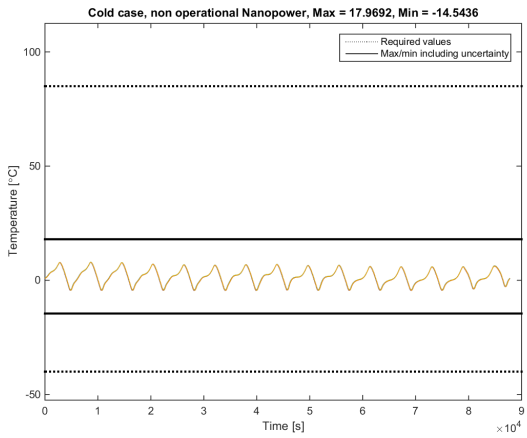

Fig. 23. Cold case, non operational Nanopower

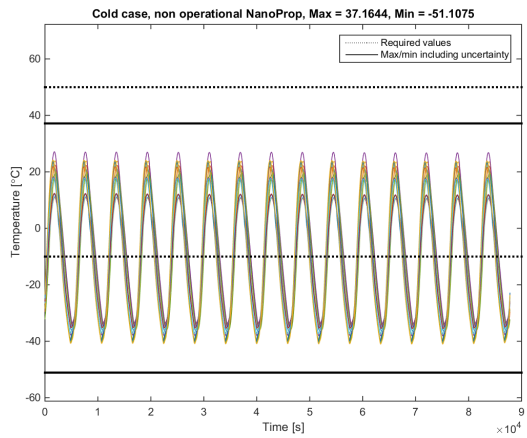

Fig. 24. Cold case, non operational NanoProp

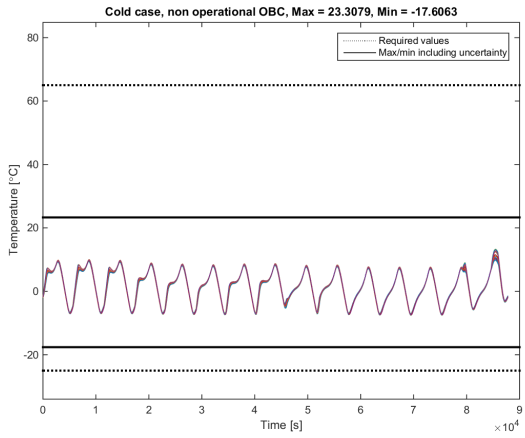

Fig. 25. Cold case, non operational OBC

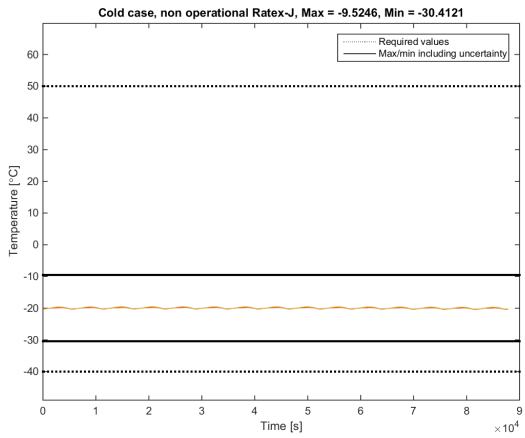

Fig. 26. Cold case, non operational Ratex-J

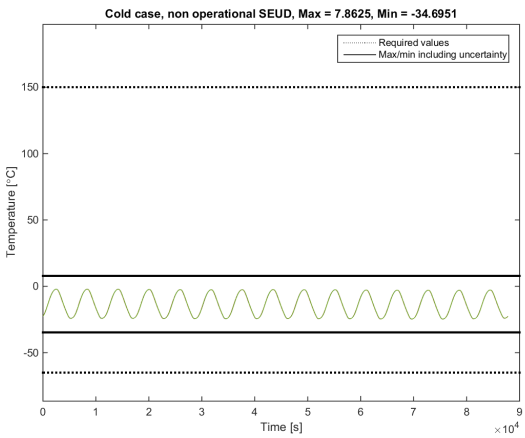

Fig. 27. Cold case, non operational SEUD

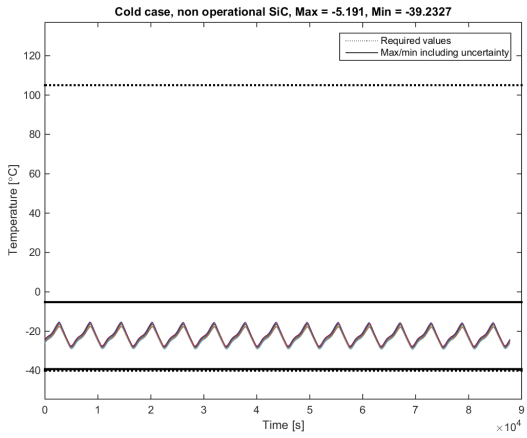

Fig. 28. Cold case, non operational SiC

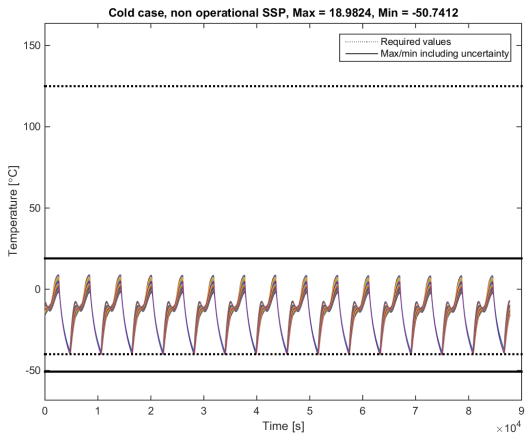

Fig. 29. Cold case, non operational Side-mounted solar panels

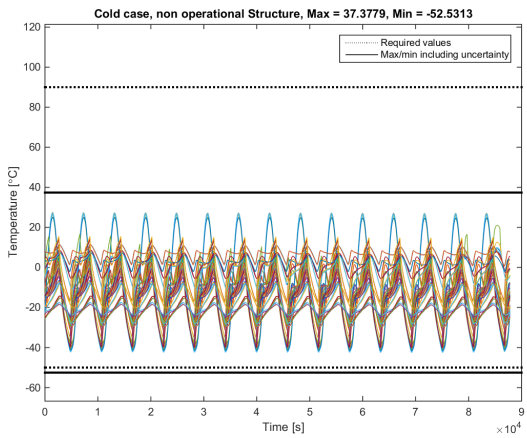

Fig. 30. Cold case, non operational Structure

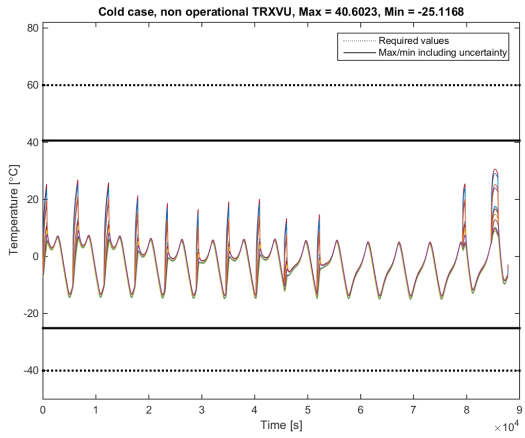

Fig. 31. Cold case, non operational TRXVU

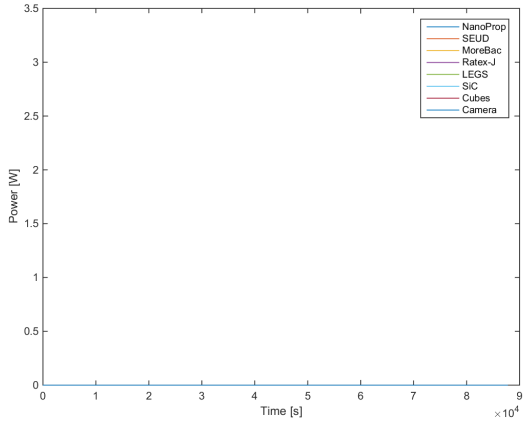

Fig. 32. Dissipation profiles, experiments, cold case, non operational

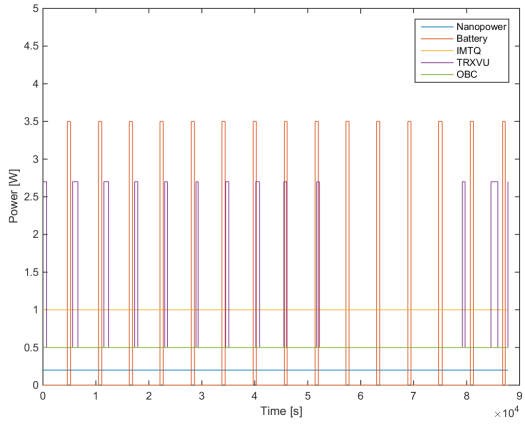

Fig. 33. Dissipation profiles, subsystems, cold case, non operational

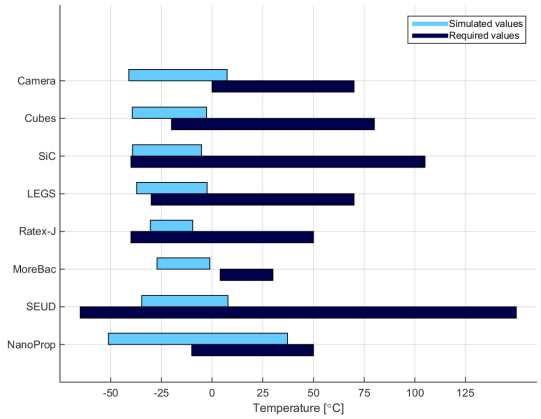

Fig. 34. Cold case, non operational, payloads

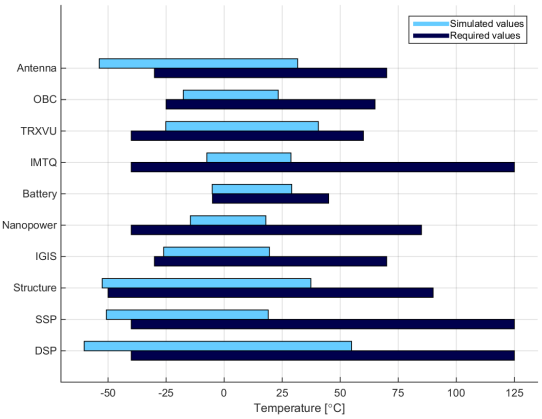

Fig. 35. Cold case, non operational subsystems

B. Cold case, operational

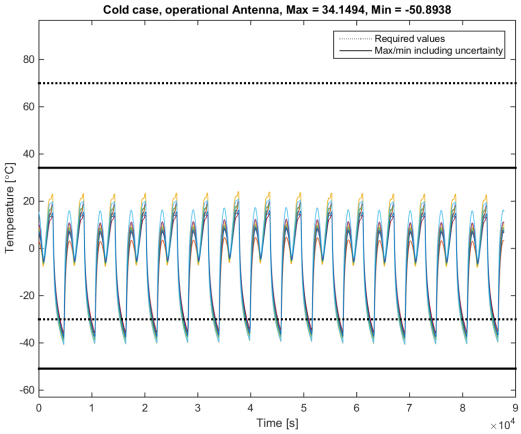

Fig. 36. Cold case, operational Antenna

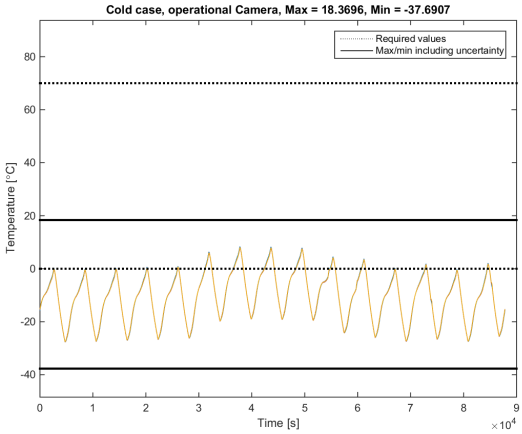

Fig. 38. Cold case, operational Camera

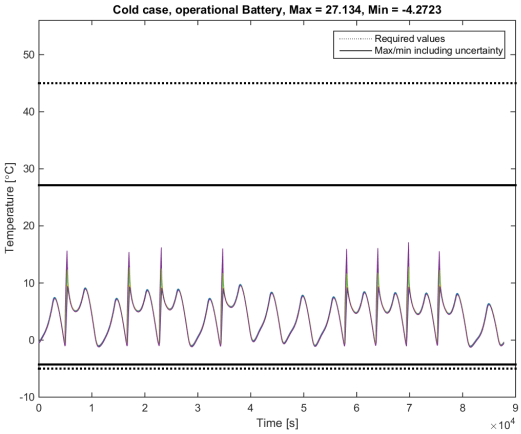

Fig. 37. Cold case, operational Battery

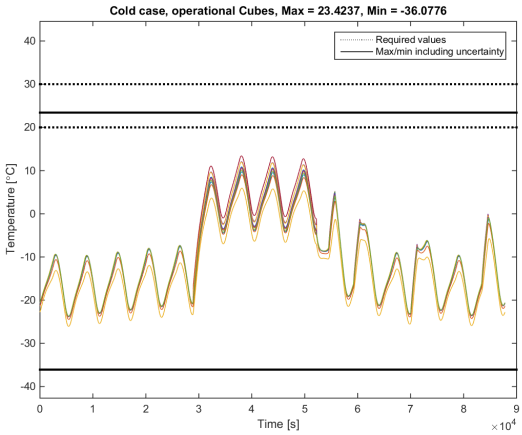

Fig. 39. Cold case, operational Cubes

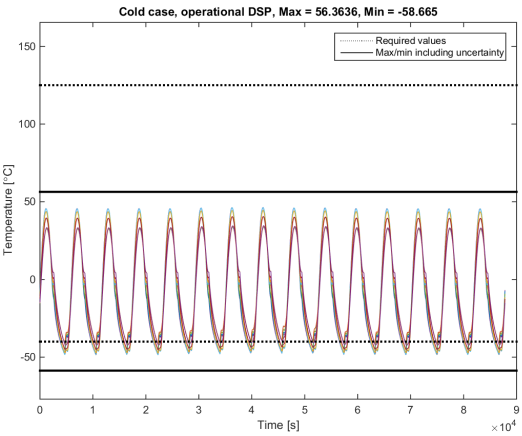

Fig. 40. Cold case, operational Deployable solar panels

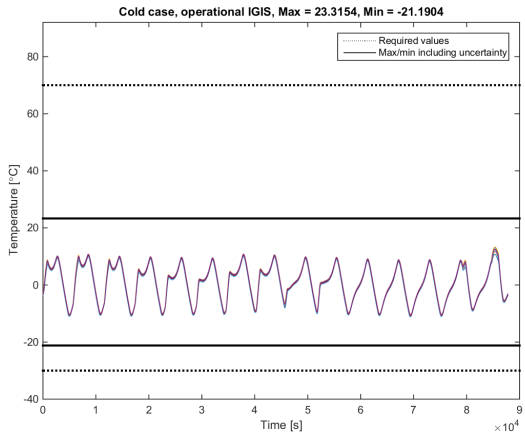

Fig. 41. Cold case, operational IGIS

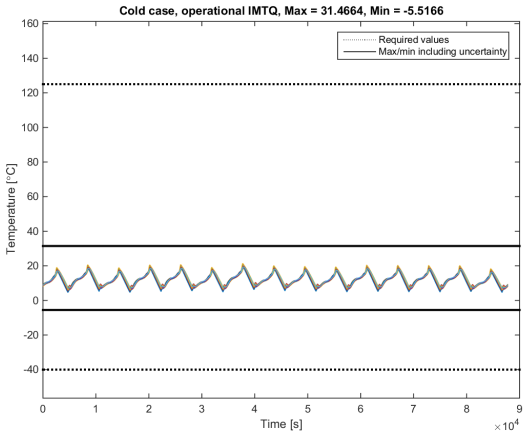

Fig. 42. Cold case, operational IMTQ

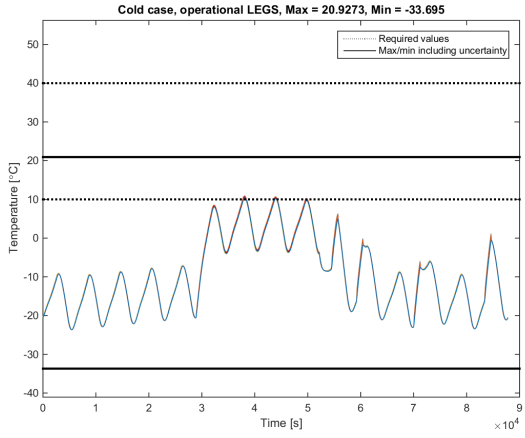

Fig. 43. Cold case, operational LEGS

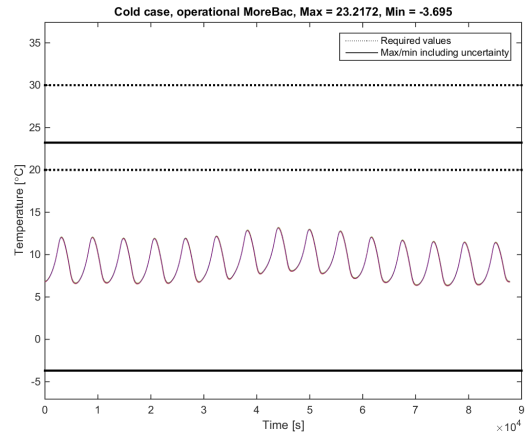

Fig. 44. Cold case, operational MoreBac

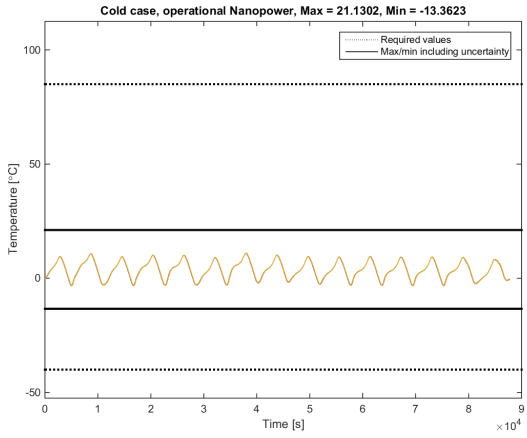

Fig. 45. Cold case, operational Nanopower

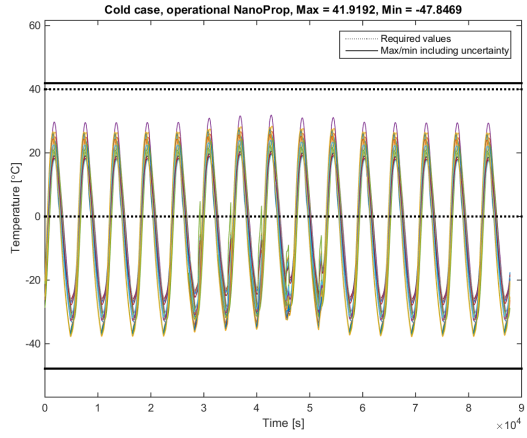

Fig. 46. Cold case, operational NanoProp

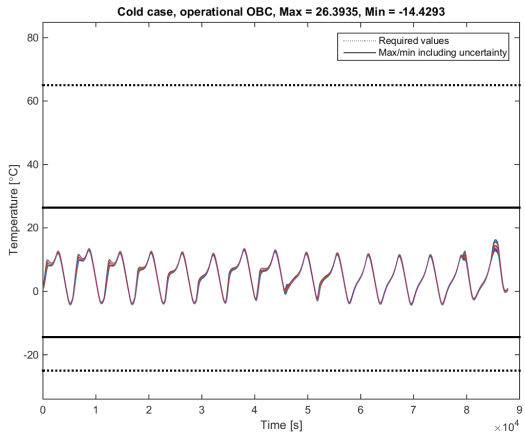

Fig. 47. Cold case, operational OBC

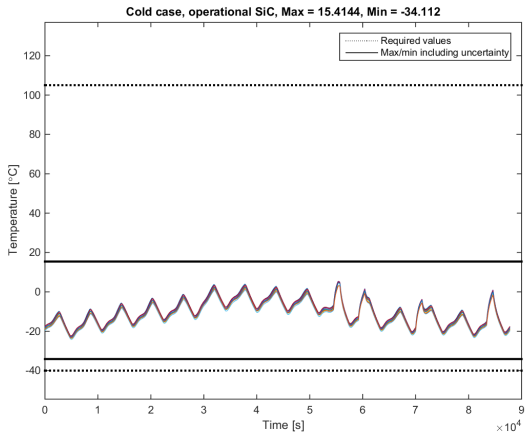

Fig. 50. Cold case, operational SiC

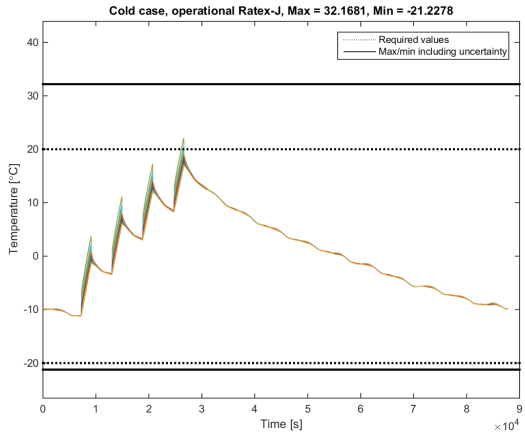

Fig. 48. Cold case, operational Ratex-J

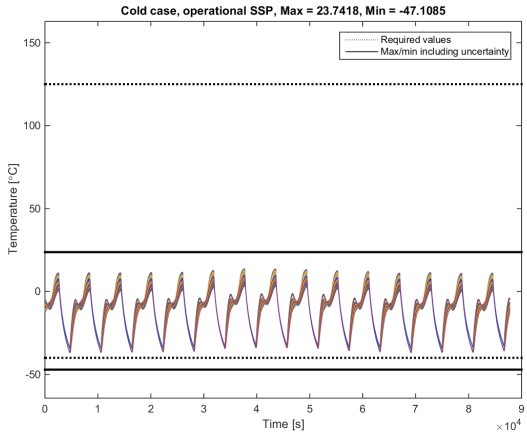

Fig. 51. Cold case, operational Side-mounted solar panels

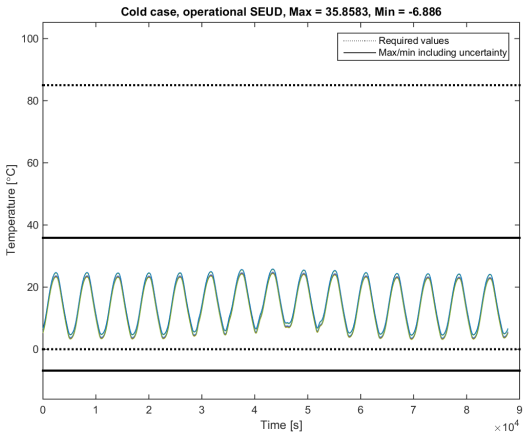

Fig. 49. Cold case, operational SEUD

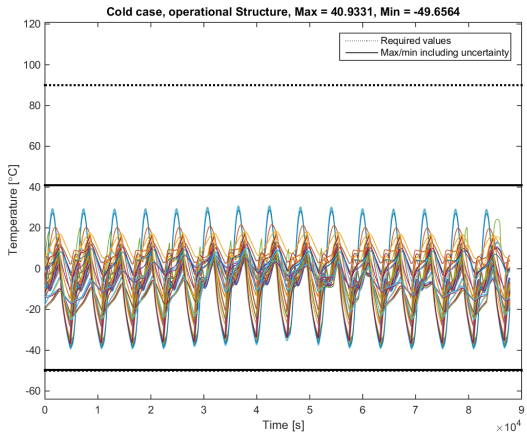

Fig. 52. Cold case, operational Structure

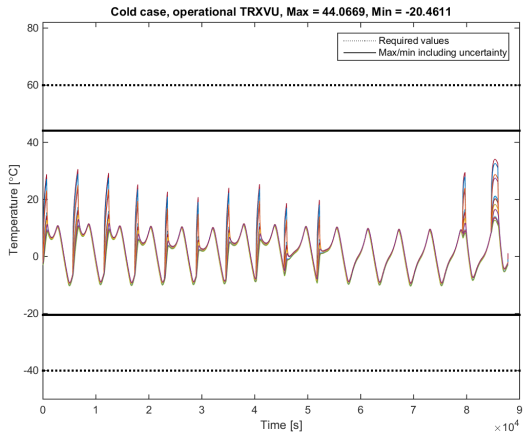

Fig. 53. Cold case, operational TRXVU

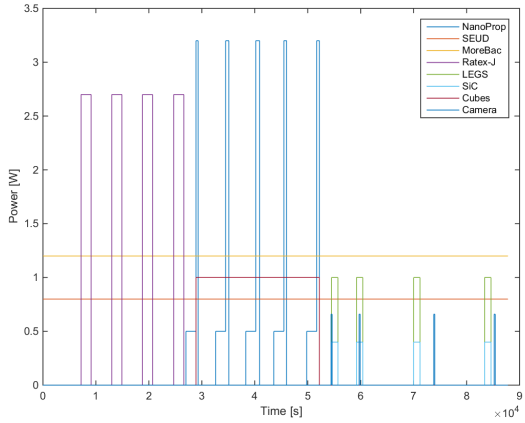

Fig. 54. Dissipation profiles, experiments, cold case, operational

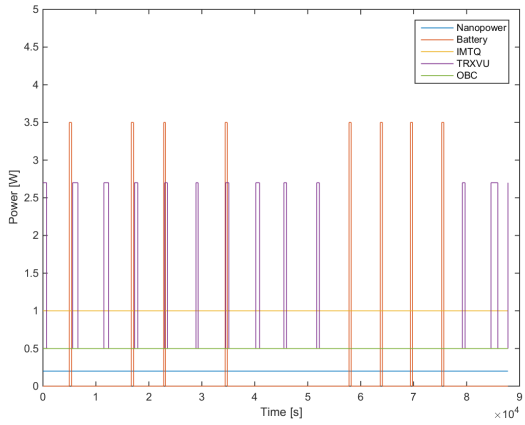

Fig. 55. Dissipation profiles, subsystems, cold case, operational

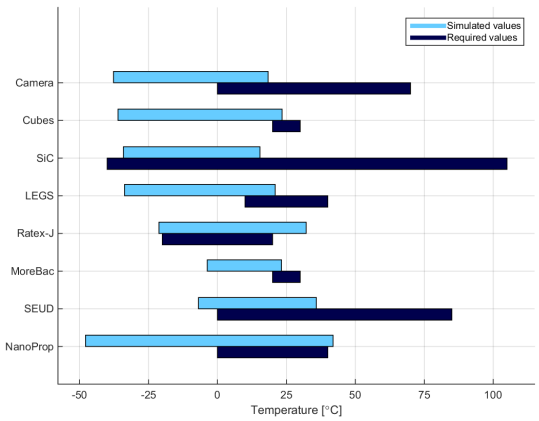

Fig. 56. Cold case, operational payloads

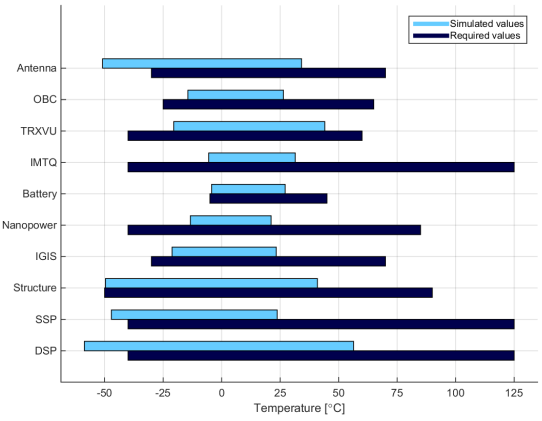

Fig. 57. Cold case, operational subsystems

C. Hot case, operational

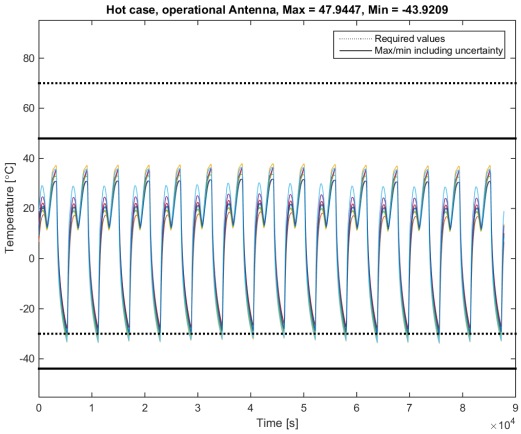

Fig. 58. Hot case, operational Antenna

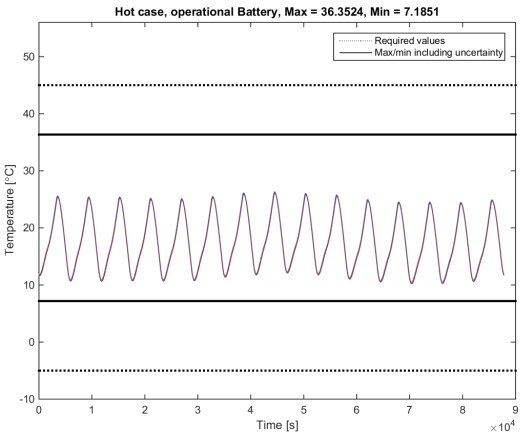

Fig. 59. Hot case, operational Battery

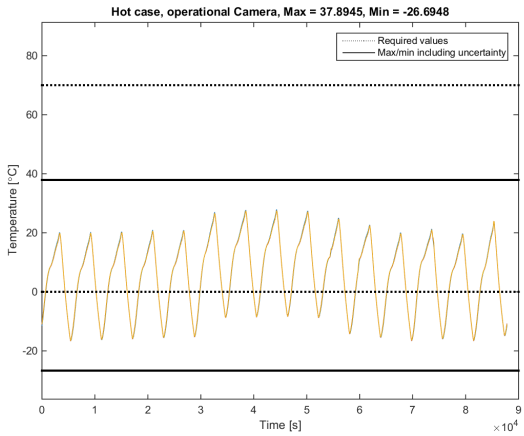

Fig. 60. Hot case, operational Camera

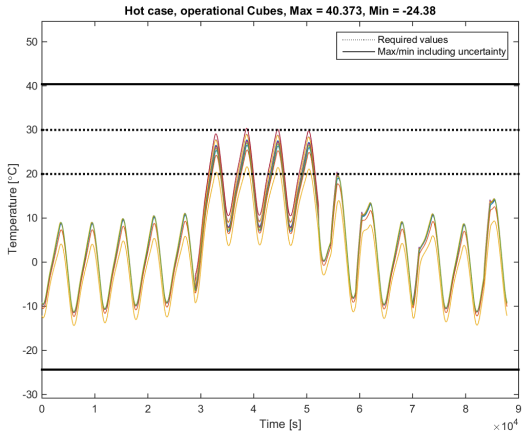

Fig. 61. Hot case, operational Cubes

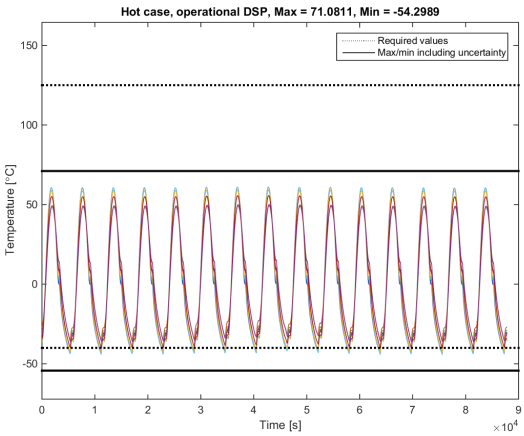

Fig. 62. Hot case, operational Deployable solar panels

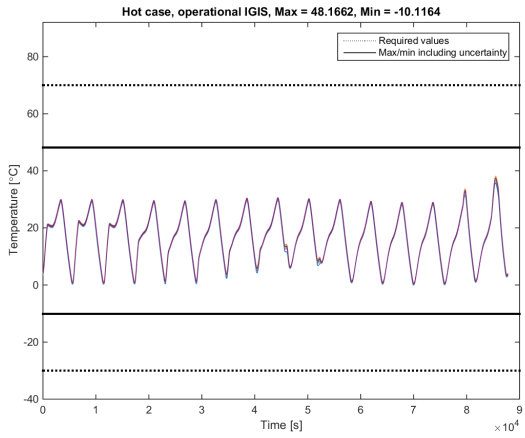

Fig. 63. Hot case, operational IGIS

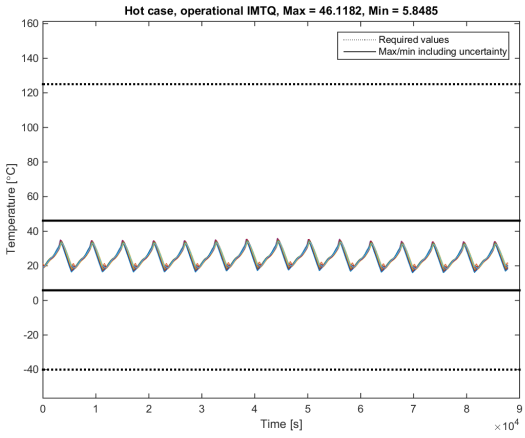

Fig. 64. Hot case, operational IMTQ

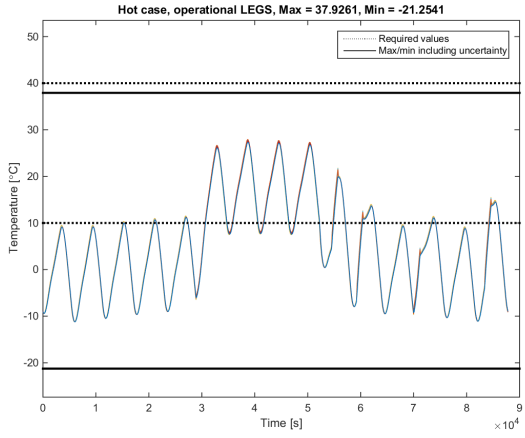

Fig. 65. Hot case, operational LEGS

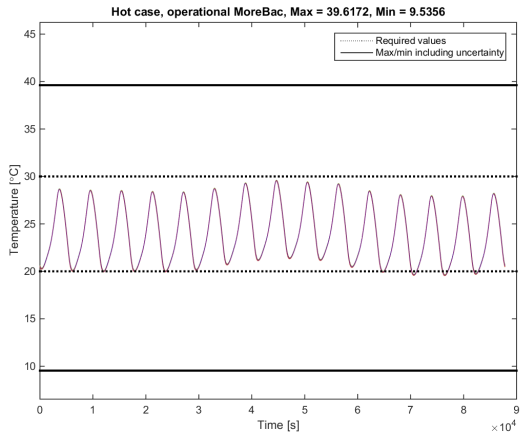

Fig. 66. Hot case, operational MoreBac

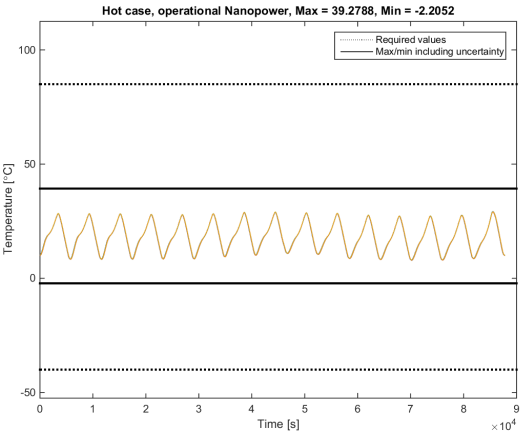

Fig. 67. Hot case, operational Nanopower

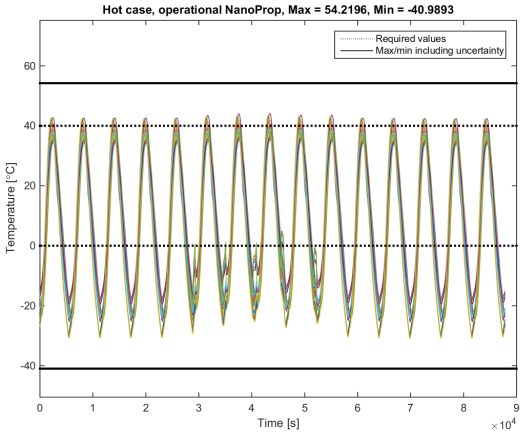

Fig. 68. Hot case, operational NanoProp

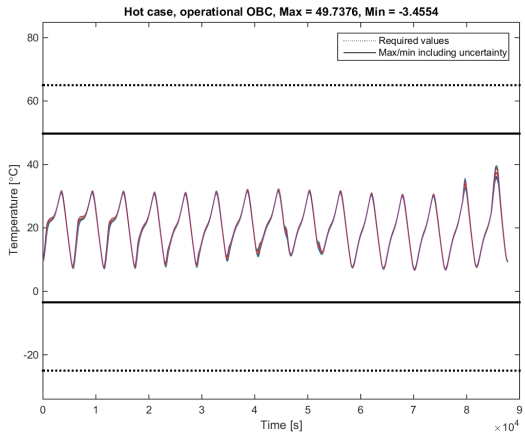

Fig. 69. Hot case, operational OBC

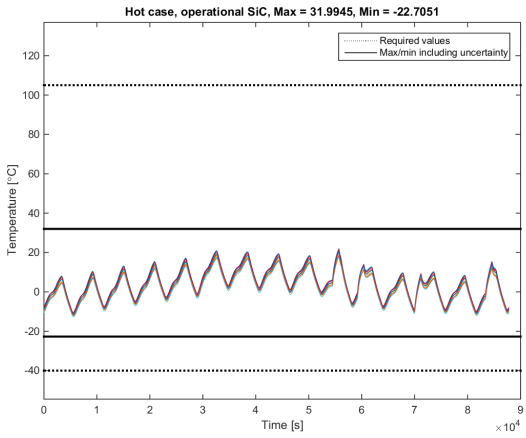

Fig. 72. Hot case, operational SiC

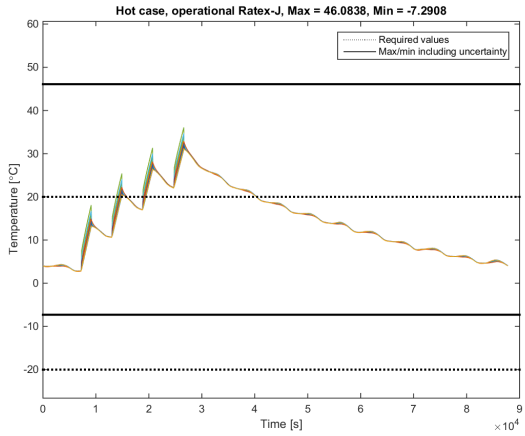

Fig. 70. Hot case, operational Ratex-J

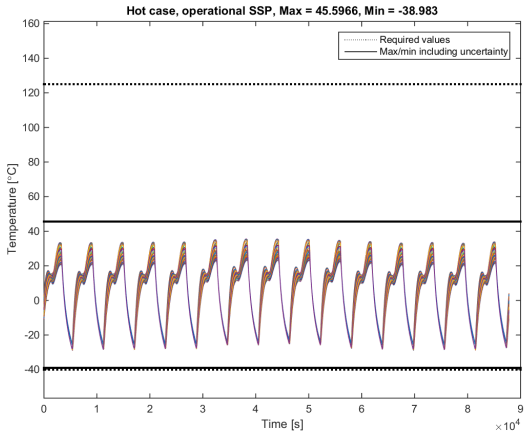

Fig. 73. Hot case, operational Side-mounted solar panels

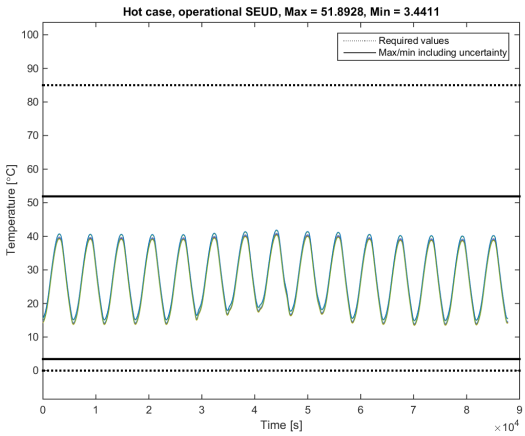

Fig. 71. Hot case, operational SEUD

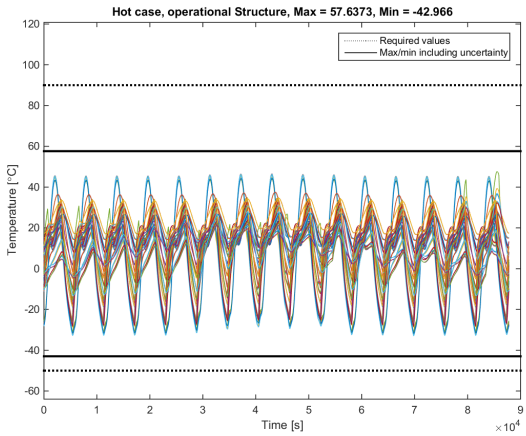

Fig. 74. Hot case, operational Structure

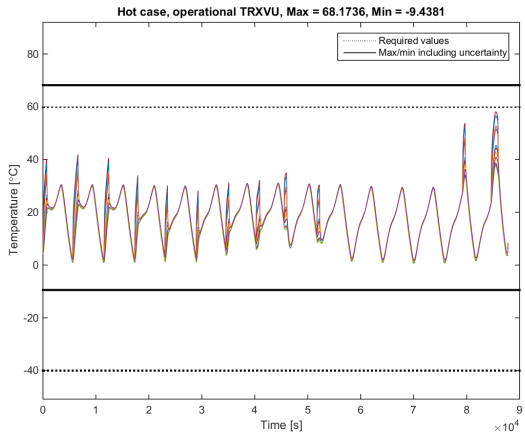

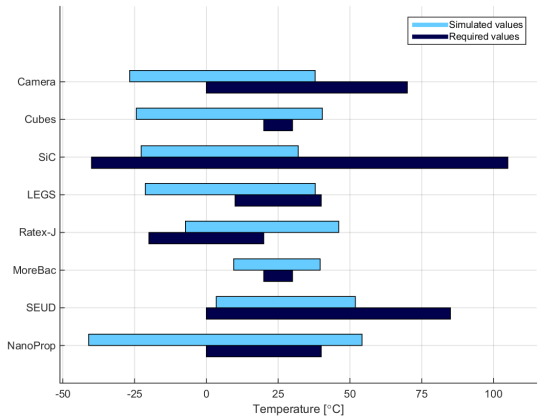

Fig. 75. Hot case, operational TRXVU

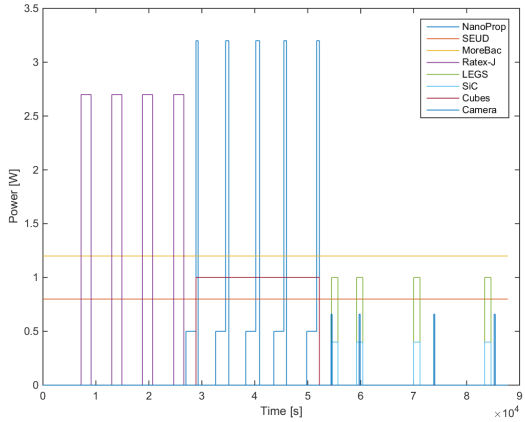

Fig. 76. Hot case, operationalDissipation profiles, experiments,

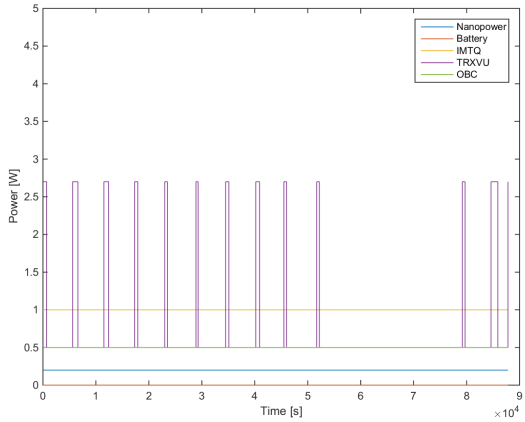

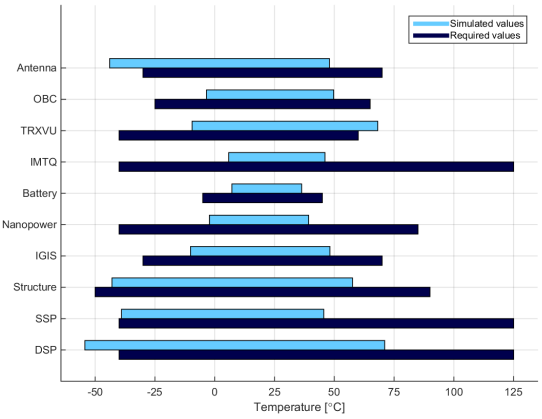

Fig. 77. Hot case, operationalDissipation profiles, subsystems,